Offshore evidence of historic and prehistoric tsunamis on the north shore of Tutuila (American Samoa)

Brieuc Riou, Eric Chaumillon, Catherine Chagué, Sabine Schmidt, Thierry Corrège, Stéphane Bujan, Jean-Luc Schneider

Journal Pre-proof

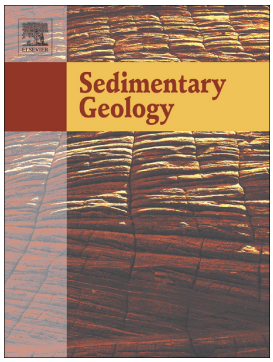

Offshore evidence of historic and prehistoric tsunamis on the north shore of Tutuila (American Samoa)

Brieuc Riou, Eric Chaumillon, Catherine Chagué, Sabine Schmidt, Thierry Corrège, Stéphane Bujan, Jean-Luc Schneider

PII: S0037-0738(23)00244-0

DOI: https://doi.org/10.1016/j.sedgeo.2023.106572

Reference: SEDGEO 106572

To appear in: *Sedimentary Geology*

Received date: 17 September 2023

Revised date: 23 December 2023

Accepted date: 26 December 2023

Please cite this article as: B. Riou, E. Chaumillon, C. Chagué, et al., Offshore evidence of historic and prehistoric tsunamis on the north shore of Tutuila (American Samoa), *Sedimentary Geology* (2024), https://doi.org/10.1016/j.sedgeo.2023.106572

Offshore evidence of historic and prehistoric tsunamis on the north shore of Tutuila (American Samoa)

Brieuc Riou[a, b], Eric Chaumillon[a*], Catherine Chagué[c], Sabine Schmidt[b], Thierry Corrège[b], Stéphane Bujan[b], Jean-Luc Schneider[b],

[a] LIENSs, UMR 7266-CNRS, Université de La Rochelle, La Rochelle CEDEX, F-17000, France

[b]EPOC, UMR-5805-CNRS, Université de Bordeaux, Pessac CEDEX, F-33615, France

[c] School of Biological, Earth and Environmental Sciences, UNSW Sydney, Sydney 2052, NSW, Australia

*Corresponding author: eric.chaumillon@univ-lr.fr

Abstract

Although research dealing with the geological evidence of past tsunamis has increased significantly in the last two decades, studies of tsunami deposits emplaced during the backwash phases are still underrepresented. Here, we provide the first investigation of tsunami backwash deposits all around an island (Tutuila Island, American Samoa), in the southwest of the Pacific Ring of Fire. We decipher the sedimentary record preserved offshore an open bay (Fagafue) and within a sheltered bay (Masefau) on the north shore of Tutuila. Backwash deposits of three historic tsunamis, namely the 2009 South Pacific, 1960 Valdivia and 1917 Tonga Trench tsunamis, were identified in sediment cores, based on sedimentological, geochemical and chronological data. Deposits were characterized by a geochemical terrestrial signature (Ti/Ca and K), while the grain size characteristics differed, being finer offshore the open bay and coarser within the sheltered bay. The 2009 South Pacific and the 1960 Valdivia tsunamis are recorded on both the north (Masefau and off Fagafue bays) and south (Pago Pago Bay) shores of Tutuila, providing the first correlation of tsunami backwash deposits all around an island. Furthermore, the present study presents the first geological evidence of backwash associated with a large 15-16th century tsunami, which also affected many parts of the South Pacific, as well as that of an older event between the 11th and 14th century. Studies of tsunami backwash deposits provide means

to extend the geological record of these high energy events, due to the generally good preservation potential of the deposits.

Keywords: tsunami; backwash deposit; core correlation; 15th century tsunami; evidence of local and far-field tsunamis.

1. Introduction

Over the last two decades, and in particular following the 2004 Indian Ocean Tsunami and the 2011 Tohoku-Oki Tsunami, research dealing with tsunamis has increased considerably (e.g., Chagué-Goff et al., 2017, their Fig. 1). This interest is motivated by the need to increase our knowledge about these events, for natural hazard assessment, and to gain a better understanding of sedimentary and geomorphologic impacts and their effects on the evolution of coastal zones. However, most studies have focused on onshore deposits while examples of geological evidence of tsunamis offshore, i.e., backwash deposits, are still underrepresented. Nevertheless, there have been a few studies dealing with backwash deposits associated with the 2004 tsunami (e.g., Sakuna et al., 2012; Sakuna-Schwartz et al., 2015), while the 2011 event led to an increased number of studies of offshore deposits and related processes (e.g., Ikehara et al., 2014, 2016, 2020, 2021; Tamura et al., 2015; Yoshikawa et al., 2015; Seike et al., 2016). Recent investigations have also been made of backwash deposits associated with historical and prehistorical events (e.g., Kümmerer et al., 2020; Smedile et al., 2020; Feist et al., 2023).

A limiting factor to the identification of event deposits in the geological record is their preservation potential. Tsunami deposits are usually emplaced in a narrow coastal band, from a few kilometers onshore (coastal plains and lagoons) to a few kilometers offshore (nearshore domain with shallow water depths) (e.g., Costa et al., 2015). Onshore deposits are particularly prone to post-depositional

changes due to natural processes but also anthropogenic activities (e.g., Szczuciński, 2020). The shoreface and, to a lesser extent, the upper offshore are highly dynamic and are often subject to intense wave erosion, currents or human activities, thus also leading to a low preservation potential (e.g., Weiss and Bahlburg, 2006; Costa et al., 2015). Previous studies have however shown that sheltered shallow marine environments provide suitable conditions for the preservation of backwash deposits (e.g., Fujiwara and Kamataki, 2007; Tamura et al., 2015; Riou, 2019; Riou et al., 2020a, 2020b). Although sediment mixing and bioturbation can also occur (e.g., Seike et al., 2016), sheltered bays are less likely to be subjected to wave effects and thus can provide a higher preservation potential (e.g., Riou et al., 2020b). In more open bays, only areas below the storm-weather wave base might provide suitable sites for the preservation of deposits (e.g. Weiss and Bahlburg, 2006). Thus, studying the geological evidence of historic and possibly paleo-tsunamis in shallow marine environments and correlating the findings with existing tsunami or earthquake reports, catalogs and databases, can help gain a better understanding of these events and extend the tsunami database. Tutuila (American Samoa), a volcanic island in the south-west Pacific (Fig. 1a), has often been struck by tsunamis originating from all parts of the Pacific Ocean, with at least four major events in the last 100 years or so, in 1917, 1957, 1960 and 2009 (Pararas-Carayannis and Dong, 1980; National Geophysical Data Center [NGDC], 2023) (Table 1). Two small tsunami waves (see Section 3) were also reported following the eruption of Hunga Tonga-Hunga Ha'apai volcano in 2022 (NGDC, 2023). The highly indented coastline of Tutuila offers numerous sheltered bays (Fig. 1b) that are ideal for the preservation of tsunami backwash deposits (Riou, 2019; Riou et al., 2020a, 2020b). A recent study in Pago Pago Bay, a sheltered bay on the south coast of the island, has shown that the two most recent major tsunamis, the 2009 South Pacific Tsunami and the 1960 Valdivia Chile Tsunami, have left discrete backwash deposits in the shallow marine sediment record (Riou, 2019; Riou et al., 2020b). Here we present a multiproxy analysis of two cores sampled in two different settings offshore the north coast of Tutuila, which was carried out in an attempt to search for evidence of the 2009 South Pacific Tsunami and possibly other tsunamis or high energy events. One core was taken within a

sheltered bay, Masefau Bay, while the other study site was in a more exposed setting, less than 1.5 km offshore Fagafue and Massacre Bays. Combined with the findings of Pago Pago Bay on the south coast of Tutuila (Riou, 2019; Riou et al., 2020a, 2020b), where the authors identified backwash deposits associated with the 2009 South Pacific Tsunami and the 1960 Valdivia Tsunami (named the 1960 Great Chilean Earthquake Tsunami in Riou et al. (2020b)), this represents the first study attempting to provide evidence of backwash deposits of an event and/or multiple events around an island.

2. Study area

The Samoan archipelago is in the south-west Pacific Ocean, at the northern end of the Tonga Trench (Fig. 1a). It is a nearly 500 km-long alignment of volcanic islands, with the oldest island in the west, Savaii, formed 5 Ma ago (e.g., Koppers et al., 2008). Tutuila is the third largest island of the archipelago and the largest of American Samoa. It was formed about 1.5 Ma ago by five coalescent shield-building volcanoes dominated by alkali olivine basalts (Hawkins and Natland, 1975), characterized by high TiO_2 and MgO but low CaO contents (Natland, 1980). The calderas formed by these volcanoes were then eroded, resulting in the current morphology of the island, with deep, narrow and sheltered bays ending in amphitheater-shaped heads with steep slopes, such as Masefau Bay (Fig. 1b). The shield volcanoes are overlain by Pleistocene post-erosional volcanic formations, dominated by olivine nephelinites and basanites (Hawkins and Natland, 1975; Natland, 1980), which are also characterized by high TiO_2 and MgO, and low CaO contents (Natland, 1980).

Fagafue Bay, on the north shore of Tutuila, is about 500 m long and 300 m wide, and is characterized by a fringing coral reef along its margin (Apotsos et al., 2011). There is a narrow alluvial valley on its eastern side, with a 10 m wide river at its mouth (Apotsos et al., 2011), but no inhabitants. Fagafue Bay, with Massacre Bay in the west and Sita Bay in the east, forms a wide-open embayment, labelled Massacre-Fagafue-Sita Bays (Fig. 1b, c). Masefau Bay is a sheltered bay located along the north shore of Tutuila, about 15 km east of Fagafue Bay. It is approximately 1.5 km long by 700 m wide and

oriented nearly perpendicular to the coastline (Fig. 1b, d). It owes its morphology only to the erosion of volcanic structures and has no major fluvial tributary. Unlike Pago Pago Bay, which is the biggest bay and location of the main harbor of the island, the head of Masefau Bay only hosts a small village along the shore.

3. Impact of historic tsunamis on Tutuila

The 2022 tsunami caused by the eruption of the Hunga Tonga-Hunga Ha'apai volcano in Tonga was recorded in Pago-Pago using tide gauges, with a 0.62 m wave followed by a smaller (0.36 m) wave (NGDC, 2023). Earlier historical tsunamis have also been reported around Tutuila (Table 1). The 2009 South Pacific tsunami was generated by an M_w 8.1 earthquake at the northern extremity of the Tonga Trench, less than 200 km off the coast of Tutuila (e.g., Okal et al., 2011). The first wave reached a maximum height of 10 m on the northern coast of Tutuila, in Poloa and Fagasa Bays, and reached a height of 5 m in Fagafue Bay and 4 m in Masefau Bay (Fig. 1b) (Fritz et al., 2011). The run-up reached nearly 18 m above sea-level (m.a.s.l.) in Poloa Bay, with 12 m.a.s.l. near Fagafue Bay and 5 m.a.s.l. in Masefau Bay (Fritz et al., 2011). Apotsos et al. (2011) also reported that the tsunami inundated nearly 250 m onshore in Fagafue Bay, mostly along the alluvial valley, with a flow depth exceeding 7 m. In Masefau Bay, Jaffe et al. (2010) measured a maximum inundation distance of 290 m.

The 1960 Valdivia (Chile) tsunami, which was generated by the most powerful historic earthquake ever instrumentally-recorded, the 1960 M_w 9.5 Valdivia earthquake, hit Tutuila with waves reaching a maximum height around 4 m in Pago Pago Bay, where a 2.4 m run-up maximum height was reported (NGDC, 2023). There were no reports on wave or run-up heights on the north coast of Tutuila (Keys, 1963; NGDC, 2023). The 1957 Aleutian Islands tsunami was generated by a M_w 8.6 earthquake in the western Aleutian Islands (Johnson et al., 1994). Maximum run-up heights reaching 1.5 m were reported in Fagasa Bay, on the north shore of Tutuila (Fig. 1b) (NGDC, 2023). The earliest of the four reported major historic tsunamis is the 1917 Tonga Trench tsunami, which was triggered by a M_w 8.7 earthquake near the northern end of the Tonga Trench, just over 200 km off Tutuila, and with an epicenter

approximately 150 km from that of the 2009 earthquake (Okal et al., 2011). The only report for the 1917 event in Tutuila is a 2.4 m high wave in Pago Pago (NGDC, 2023). Very little to no reports of tsunamis affecting Tutuila prior to 1917 were found, except for a 0.60 m wave reported in Pago Pago that was due to a tsunami caused by the 1837 Ms 8.5 Chile earthquake (NGDC, 2023). Sedimentological records of tsunamis prior to the 1960 Chile tsunami are indeed still rare in the Samoan Islands (Williams et al., 2011a, 2011b, 2020).

4. Material and methods

4.1. Fieldwork and bathymetry

This work was completed following the acquisition of a large and exhaustive marine dataset from the SAMOA-SPT oceanic campaign around the island of Tutuila. This campaign, carried out between August 27th and September 10th 2015 aboard the *R/V Alis*, included bathymetric, seafloor reflectivity and very high-resolution seismic surveys, and sediment core sampling (Schneider, 2015).

Seafloor bathymetry was acquired using an EM1002 multibeam echo-sounder (Kongsberg Maritime), with a frequency of 95 kHz. The depth range covered by this device is from 5 to 1000 m, which is appropriate for coastal zones. A raw bathymetric survey of approximately 75 km² was obtained on the north coast of Tutuila, covering most bays including Masefau Bay, and the area just offshore Massacre, Fagafue and Sita Bays. Raw data were processed using the CARAIBES (CARtography Adapted to Imagery and BathymEtry of Sonars and multibeam echo-sounders) software developed by IFREMER. This signal processing consisted of tide and wave corrections, followed by elimination of bias due to irrelevant celerity variations in the water column. The processed data were then exported as a 1 m resolution DEM (Digital Elevation Model).

A total of eleven cores were collected in Masefau Bay and offshore Massacre-Fagafue-Sita Bays (the latter referred below as off Fagafue Bay) (Table 2). Two different devices were used for this purpose. In each study area, three Kullenberg cores and two or three short interface cores taken using a hand-held manual corer were retrieved (Table 2). The Kullenberg coring system uses a piston allowing

greater penetration in soft sediment, while the hand-held manual corer is driven by divers and has a maximum penetration of a few tens of centimeters. The core locations were selected in the deepest parts of each bay (Fig. 1c, d), where sediment preservation, below the fair-weather wave base, was supposed to be maximum. Core K08 was sampled in a small trough at 50 m water depth, inferred to offer a sheltered hydrodynamic setting near the seafloor, beyond the fair-weather wave base, about 1.2-1.5 km off Fagafue Bay (Fig. 1c). In Masefau Bay, core K16 was sampled at 44,5 m water depth, at the seaward edge of the bank evidenced by the sea-floor bathymetry analysis (Fig. 1d). These two cores (150 cm-long Kullenberg cores) were selected for further analysis, based on the coring site location and morphologic characteristics, grain size and observable sedimentological pattern.

4.2 Analytical methods

4.2.1 Sedimentological and geochemical analysis

All cores were split in one working half and one archive half, photographed (Figs. S1-S4, supplementary material) and logged. Grain size analysis was conducted on the two selected cores. Sediment samples were collected every centimeter and analyzed using a Malvern Mastersizer S laser particle size analyzer (Malvern Analytical Ltd.). There was no pretreatment except sieving in a few layers to remove particles larger than 1250 μm. These larger particles were however rare. Statistical analysis was performed using the arithmetic method of moments with the Gradistat 8.0 software (Kenneth Pye Associates Ltd.) (Blott and Pye, 2001). The grain size distribution was plotted using a MATLAB routine developed at the University of Bordeaux.

Geochemical analysis was carried out with a XRF (X-Ray Fluorescence) core scanner (Avaatech XRF Technologies). Two runs per core were made with a 1 mm measuring step in order to obtain the full element spectrum. The first run was set at 10 kV and 1500 μA (light elements) and the second run at 30 kV and 2000 μA (heavy elements). However, here, we only present the results for selected elements, namely titanium over calcium (Ti/Ca) and potassium (K), as they are most likely to provide insights into the sediment sources in these cores (Riou et al., 2020a, 2020b). The chemical

composition of the volcanic rocks of Tutuila is characterized by high titanium and low calcium contents (Hawkins and Natland, 1975; Natland, 1980; Morrison et al., 2010), while the marine seafloor sediments in bays around the island are dominated by calcium (Morrison et al., 2010). Thus their distribution, but in particular the ratio Ti/Ca, is likely to help distinguish the terrestrial vs marine source of sediment, as shown in previous studies in Pago Pago Bay (Riou et al., 2020a, 2020b) or Upolu, Samoa (Chagué-Goff et al., 2017). In addition, potassium normalized to the total number of counts (K_{norm}) is also used here as a tracer for basaltic material from the land, as also reported by Morrison et al. (2010), who measured major and trace elements concentrations in surface marine sediments from a number of bays around Tutuila. K is also often used as a marker for clay and as an indicator of fine sediment (e.g., Cuven et al., 2013; Chagué-Goff et al., 2017; Chagué, 2020).

4.2.2 Chronology

4.2.2.1 ^{14}C dating

A total of six samples were collected from both cores and dated at the Accelerator Mass Spectrometry (AMS) facility of the Poznan Radiocarbon Laboratory (Poznan, Poland) (Table 3). Dated samples were of three types and included *Halimeda* (algae) calcified plates, benthic foraminifers and plant debris (Fig. 2). When possible, samples were collected above and below what was interpreted as anomalous or event layers, based on the elemental profiles. Results were first provided as conventional ages either as years BP (Before Present) for samples older than 1950 or in pMC (present Modern Carbon) for the sample younger than 1950 (Table 3). For samples older than 1950, the age calibration was achieved using the Calib rev.8 software (http://calib.org/calib/, Stuiver and Reimer 1993) coupled with the Marine20 calibration curve (Heaton et al. 2020). This curve applies a global age correction of about 400 years to take into account the reservoir effect of marine samples. A local component ΔR is added to this global reservoir age correction to reflect the local variations such as deep ocean upwelling or other local effects. Here, a ΔR of -143 $\pm$ 20 years was used from samples located in Tutuila Island, Pago Pago (Petchey et al., 2008). For the plant debris, the calibration was made using

the Postbomb curve (Reimer and Reimer, 2023). All ^{14}C ages in this study are calibrated and expressed as calendar years (CE), and are given as an interval corresponding to the 95% confidence interval (2 sigma, Table 3). Only one sample could not be calibrated (SPT24).

4.2.2.2. ^{210}Pb and ^{137}Cs dating

The age models of the two Kullenberg cores over the last century were based on excess ^{210}Pb ($^{10}Pb_{xs}$; $T_{1/2}$ = 22.3 years) and ^{137}Cs ($T_{1/2}$ = 30 years) depth profiles. Activities of ^{210}Pb, ^{226}Ra, ^{232}Th and ^{137}Cs of sediment samples (n = 27) were determined by gamma spectrometry using a Broad Energy germanium detector calibrated using IAEA reference material (Schmidt and De Deckker, 2015). The coarse carbonate fraction was removed by sieving (63 μm mesh size) to avoid changes in activities due to dilution. Activities are expressed in mBq g^{-1} and errors are based on one standard deviation counting statistics. Excess ^{210}Pb was calculated by subtracting the activity supported by its parent isotope, ^{226}Ra, from the total ^{210}Pb activity in the sediment. Sediment layers were measured downcore until a negligible excess was reached. Mean sedimentation rates (SAR) were calculated assuming constant flux and constant sedimentation (referred to as the CF:CS model; Krishnaswamy et al., 1971).

5. Results and interpretation

5.1 Sea-floor bathymetry

Massacre-Fagafue-Sita Bays represent an open bay (Fig. 1c), protected from ocean waves and currents only by the outer reef barrier. In the shallow nearshore part of the bays, down to the 35 m isobaths, a few mounds, likely reef mounds, are present. Less than 1 km off the coast, there is a west-east oriented ca. 1.5 km long, 500 m wide and 5-10 m deep (relative to the surrounding seafloor) trough (Fig. 1c). This small depression reaches a water depth of about 50 m and is limited to the south by the Massacre-Fagafue-Sita Bay sediment fill and to the north by a west-east-trending ridge, culminating at 37 m water depth (Fig. 2c). Based on the results of the bathymetric survey, we selected the

depression as the site to sample the sediment cores, as it is likely to offer a better preservation potential than other shoreface areas with a regular slope toward the ocean.

Unlike Massacre-Fagafue-Sita Bays, Masefau Bay is a very narrow and more sheltered bay (Fig. 1d). At the mouth of the bay, a 5-10 m bathymetric high isolates the inner bay from the outer bay, delineating a small basin in the bay, ideal for sediment preservation on the seafloor. In the inner part of the bay, the seafloor morphology is marked by a bank suggesting a prograding sediment-fill. This bank is interrupted by a few mounds, most likely reef mounds, down to 45 m depth.

5.2 Cores

5.2.1 Stratigraphy and grain size

Visually, core K08 (off Fagafue Bay) appears composed of relatively homogeneous silty to sandy sediment, with slightly darker intervals found around 13-18 cm and 71-85 cm depth (Figs. 3, S1, S2 in supplementary material). Visually, no internal structures were observed. Some vascular plant debris could however be seen at 13 cm depth (Fig 2a). Despite the visual homogeneous-looking sediment, grain size distribution obtained from laser microdiffractometry reveals major grain size variations throughout the core and the sediment is generally poorly to very poorly sorted (Tables 4, S1 in supplementary material). The mean grain size varies between about 100 and 350 µm, with a few slightly finer-grained units identified between about 13-18 cm, 23.5-26 cm and 71-85 cm depth (Fig. 3, Tables 4, S1 in supplementary material). These finer-grained units also often exhibit normal or inverse grading (Table 4).

Unlike core K08, sediment within core K16 appears less homogenous visually. Slightly darker sediment can be seen around 5-20 cm and 115-122 cm depth (Figs. S3, S4, supplementary material). Grain-size distribution displays coarser sediment at the top (0-20 cm) and alternation of bimodal very poorly sorted sediment (63-75 cm and 93-115 cm depth) with relatively better sorted sediments (20-63 cm, 75-83 cm, 87-115 cm, 115-119.5 cm) (Fig. 4, Tables 4, S2 in supplementary material). In addition, abundant *Halimeda* plates are mixed with this better sorted sediment, while they are rare in the coarser intervals.

Visually, no internal structures were observed, but inverse grading was recorded, based on grain size analysis, in at least one of the anomalous layers (Tables 4, S2 in Supplementary material).

5.2.2 Geochemistry

In core K08, the Ti/Ca ratio and K_{norm} distribution display a generally similar trend, with higher values at 13-18 cm, 23.5-26 cm, 71-85 cm and 105-112 cm depth, although it is very subtle in the latter for K_{norm}. These higher values generally also correlate with a finer mean grain size at these depths and exhibit sharp increases at 18 cm and 26 cm depth (Fig. 3).

In core K16, there are only two intervals at 113-120 cm and 136-139 cm depth, where Ti/Ca and K_{norm} display marked increases, with the lower one more or less correlated with change in mean grain size (Fig. 4). In the remaining of the core, Ti/Ca and K_{norm} profiles show little variation

5.2.3 Identification of anomalous layers

Based on the distribution of Ti/Ca and K_{norm} and the grain size characteristics, as well as additional sedimentological characteristics, such as reverse or normal grading (but not always), a number of units were identified, which differ from the background sediment in the cores. In the following, we label them anomalous layers (AL, with the code of the core in subscript), and describe them from the top of the cores downward, and this for each core.

5.2.3.1 Core K08, off Fagafue Bay

In core K08, four anomalous layers were identified (Fig. 3, Table 4) as follows:

The first one, $AL1_{08}$, between 13 and 18 cm depth, is marked at its base by an increase in Ti/Ca and K_{norm} counts. It consists of unimodal, poorly to very poorly sorted sandy mud (mean grain size between 72 and 137 μm; sorting between 113 and 192; skewness between 2.48 and 5.186; kurtosis between 10.14 and 36.37) (Table S1) exhibiting a normal grading, with higher K_{norm} counts and Ti/Ca ratio. The sediment in this layer is finer, more poorly sorted and of a darker color compared to the underlying

and overlying sediment. There is also some vascular plant debris at the top of this unit, at 13 cm depth.

The second one, $AL2_{08}$, between 23.5 and 26 cm depth, consists of unimodal, very poorly sorted sandy mud (without any grading) (mean grain size between 86 and 94 μm; sorting between 122 and 132; skewness between 2.85 and 3.12; kurtosis between 12.62 and 14.85) (Table S1), and is also more poorly sorted than the background sediment (Fig. 3). It is characterized by a marked increase in K_{norm} counts at its base, and higher K_{norm} counts and Ti/Ca ratio than the overlying and underlying sediment. There is however no change in color.

The third one, $AL3_{08}$, between 71 and 85 cm depth, consists of unimodal, very poorly sorted sandy mud with muddy sand at the base and top (mean grain size between 45 and 158 μm; sorting between 68 and 260; skewness between 2.08 and 4.41; kurtosis between 7.64 and 28.22) (Table S1), with a marked but gradual increase in Ti/Ca and K_{norm} counts at the base, which correlates with a gradual decrease in grain size (compared to the underlying sediment) and sorting (Fig. 3). The sediment of $AL3_{08}$ fines upward (normal grading) then coarsens upward (reverse grading) and is darker than the background. It is also more poorly sorted.

- The fourth one, $AL4_{08}$, between 103.5 and 112.5 cm depth, is mostly marked by an increase in Ti/Ca correlating with an alternation of bimodal and unimodal poorly to very poorly sorted muddy sand (mean grain size between 98 and 332 μm; sorting between 132 and 467; skewness between 1.74 and 4.28; kurtosis between 4.99 and 27.72) (Table S1) exhibiting a subtle reverse grading. Although the grain size variations do not show major changes compared to those in the overlying and underlying sediment, the sediment is more poorly sorted, as reported for the other anomalous layers. K_{norm} counts show a marked decrease at the upper boundary of the layer.

5.2.3.2 Core K16, Masefau Bay

In core K16, five anomalous layers were identified (Fig. 4, Table 4), mostly (but not always) based on the difference in grain size distribution.

The first one, $AL1_{16}$, between 7 and 20 cm depth, consists of very poorly sorted muddy sand displaying an alternation of layers with bimodal and unimodal grain size distribution, and two fining-upwards sub-units, with a thin coarser interval at 10-12 cm depth (mean grain size between 125 and 390 μm; sorting between 146 and 503; skewness between 1.03 and 2.80; kurtosis between 3.45 and 11.39) (Table S2). A sharp lower contact with the finer underlying sediment, while not easy to see with the naked eye, was recorded using grain size analysis. Only rare *Halimeda* plates occur in this layer. While Ti/Ca distribution does not exhibit any changes with the underlying sediment, the ratio displays a small but marked decrease at the upper boundary of this unit. K_{norm} distribution shows some variation.

The second one, $AL2_{16}$, between 35.5 and 40 cm depth, consists of trimodal, bimodal and unimodal poorly to very poorly sorted sandy mud with muddy sand at the top (inverse grading) (mean grain size between 64 and 253 μm; sorting between 100 and 377; skewness between 2.07 and 4.36; kurtosis between 7.01 and 26.34) (Table S2), with two small coarser intervals, compared to the background sediment (Fig. 4). There are also only a few *Halimeda* plates in this layer.

The third one, $AL3_{16}$, between 60 and 75 cm depth, displays a very poorly sorted (mostly bimodal grain size distributions) sandy mud and muddy sand with a sharp base (mean grain size between 99 and 364 μm; sorting between 153 and 462; skewness between 1.39 and 2.93; kurtosis between 4.24 and 13.07) (Table S2). A few *Halimeda* plates are found in this layer. As in $AL2_{16}$, the Ti/Ca and K_{norm} profiles do not display any major changes from the background.

The fourth one, $AL4_{16}$, between 93 and 119.5 cm depth, stands out due to the very high Ti/Ca and K_{norm} counts and sharp increase at the base of the layer (113-119.5 cm depth). Ti/Ca and K_{norm} counts are also higher than in the overlying and underlying sediment. This layer is darker than the background and consists of bimodal very poorly sorted sandy mud with thin intercalations of muddy sand, and a sharp basal contact (mean grain size between 88 and 299 μm; sorting between 161 and 385; skewness between 1.42 and 3.09; kurtosis between 4.92 and 13.16) (Table S2). There are only a few *Halimeda* plates in this layer.

The fifth one, $AL5_{16}$, between 135 and 139.5 cm depth, consists of bimodal very poorly sorted sandy mud (mean grain size between 82 and 324 μm; sorting between 149 and 354; skewness between 1.348 and 3.056; kurtosis between 4.351 and 12.46) (Table S2). This layer is different from the other anomalous layers in core k16 in that it is characterized by a finer sediment than the background and it also displays a small peak in both Ti/Ca and K_{norm} counts (in the lower part of $AL5_{16}$).

5.2.4 Chronology

The chronology of the two sedimentary sequences was established using ^{210}Pb, ^{137}Cs and ^{14}C. In core K08, the $^{210}Pb_{xs}$ profile can be divided into three domains (Fig. 3). In the uppermost layer (0 - 4 cm), the activity is the highest (270 $mBq.g^{-1}$). Then, between 4 and 17 cm depth, the activities are much lower (around 140 – 150 $mBq.g^{-1}$) and even increase slightly downcore, although this occurs within the top two identified anomalous layers, $AL1_{08}$ and $AL2_{08}$. From the base of $AL2_{08}$, $^{210}Pb_{xs}$ shows an exponential decrease downcore to 50 cm depth. Below 60 cm depth, activities are negligible (5 $mBq.g^{-1}$). The $^{210}Pb_x$ profile section between 18 and 50 cm depth is then used to estimate the sedimentation rate in this part of the core. The fairly constant ^{232}Th activities (a long-lived and naturally-occurring radionuclide usually associated with the detrital fraction) around 5 $mBq\ g^{-1}$ (Fig. 3) in this section indicate the absence of changes in lithological sources, implying that the changes with depth of $^{210}Pb_{xs}$ activity are mainly related to the radioactive decay of ^{210}Pb. Thus, assuming constant flux and constant sedimentation (referred to as the CF:CS model; Krishnaswamy et al., 1971), the mean sedimentation accumulation rate (SAR) was estimated to be 0.51 ± 0.04 $cm.yr^{-1}$ (Fig. 3). The deposition time of each sediment layer, in years and excluding the anomalous layers, was estimated by dividing the depth by the mean SAR, assuming the top of the core to be 2015 (date when the cores were sampled). This age vs depth model was then corroborated using the ^{137}Cs activity (Fig. 3), although the potential mobility of ^{137}Cs in saline sediments should also be considered (e.g., Hancock et al., 2011). ^{137}Cs activity is very low, as also observed elsewhere in the Southern Hemisphere, including the Samoan Islands (Terry et al., 2006; Riou et al., 2020b). However, there is a small maximum at 20 cm depth, which we ascribe to

the maximum atmospheric fallout (1964-1965) in the Southern Hemisphere (e.g., Terry et al., 2006; Riou et al., 2020b). In addition, four radiocarbon ages were obtained in this core (Fig. 3, Table 3): 1960-1962 −1985-1987 CE (modern) near the top of $AL1_{08}$ (13 cm depth), 1416-1663 CE immediately above $AL3_{08}$ (69 cm depth) and 1960-1962 −1985-1987 CE 1-1751 CE below this layer (83 cm depth), and 1031-1290 CE below $AL4_{08}$ (125 cm depth).

In core K16, $^{210}Pb_{xs}$ activities are around 113 mBq.g^{-1} and remain constant in the top 20 cm, which include the anomalous layer $AL1_{16}$, thus suggesting mixing (if there was not any mixing, the $^{210}Pb_{xs}$ activities would decrease). Below 20 cm depth, $^{210}Pb_{xs}$ displays a regular exponential decrease (except for lower activities in $AL2_{16}$ and $AL3_{16}$), which is associated with a fairly constant ^{232}Th, around 2.6 mBq g^{-1} (Fig. 4). As for core K08, we retained the sections of the profiles below layer $AL1_{16}$ to estimate a mean sedimentation rate of 0.69 ± 0.16 cm.yr^{-1} using the CF:CS model. The peak of ^{137}Cs activity at 34 cm depth (1964-1965 CE), immediately above $AL2_{16}$, validates the age depth $^{210}Pb_{ex}$ model (Fig. 4). One radiocarbon age was obtained (Fig. 4, Table 3) 1433-1677 CE below $AL4_{16}$ (125 cm depth).

6. Discussion

6.1 Origin of anomalous/event layers

Mostly based on sedimentological and chemical characteristics, four and five anomalous layers were identified in cores K08 (off Fagafue Bay) and K16 (Masefau Bay), respectively (Figs. 3, 4; Table 4; Section 5.2.3). The environmental settings are different, with core K08 taken in a small trough offshore Fagafue Bay, while K16 was taken in a sheltered bay.

Due to the more open morphology, Fagafue Bay is more exposed to waves compared to Masefau Bay. In such a setting, the background sediment in core K08 (off Fagafue Bay) exhibits large mean grain size variations and is generally much coarser than that of the anomalous layers ($AL1_{08}$, , $AL2_{08}$, $AL3_{08}$, $AL4_{08}$, Fig. 3), although the sediment in these (anomalous) layers is not as well sorted. All anomalous layers exhibit higher Ti/Ca and K_{norm} counts than in the background sediment. Based on these characteristics, the anomalous layers are interpreted as event deposits, with their Ti/Ca composition suggesting a

dominant terrestrial source. As reported in previous studies (e.g., Natland, 1980; Morrison et al., 2010; Chagué-Goff et al., 2017), high Ti and K are attributed to the basaltic rocks dominating the Samoan islands, with K also often associated with clays and other fine-grained sediment, derived from weathering of basaltic rocks, while Ca reflects the carbonates and corals offshore and in bays around the islands (e.g., Morrison et al., 2010; Chagué-Goff et al., 2011, 2017). A similar pattern of Ti vs Ca distribution has been reported from other studies elsewhere, including offshore Khao Lak, Thailand (Sakuna et al., 2012) and in the Mediterranean (Smedile et al., 2020). The thin veneer of plant debris at the top of $AL1_{08}$ also suggests a terrestrial source for the layer. Similarly, Feist et al. (2023) reported an increase in terrigenous material at the top of event layers on the Algarve Shelf off the coast of Portugal. What is however different from most other high-energy deposits in offshore settings is that the background sediment is usually finer (e.g., Fujiwara and Kamataki, 2007; Sakuna et al., 2012; Sakuna-Schwartz et al., 2015; Tamura et al., 2015; Yoshikawa et al., 2015; Riou et al., 2020a, 2020b; Smedile et al., 2020; Feist et al., 2023), as opposed to what is observed off Fagafue Bay. This is most probably attributed to the more exposed environmental setting 1.5 km off Fagafue Bay. Indeed, the shoreface sediment located offshore this bay can be affected by waves propagating from the Pacific Ocean, with wavelengths longer than 100 to 200 m (Collard et al., 2009). Such long gravity waves are likely to rework the shoreface at a few tens of meters water depth, resulting in relatively coarse sedimentation (mainly material) relative to sheltered bays protected from ocean waves. The sheltered Pago Pago Bay with its silty sedimentation represents a good example of the latter this type of depositional environment.

In Masefau Bay (core K16), the background sediment consists mostly of very well to well sorted coarse silt, while the anomalous layers are characterized by poorly sorted fine to medium sand, except in $AL5_{16}$ near the base of the core, which consists of very fine sand. In this core, only two of the layers ($AL4_{16}$ and $AL5_{16}$) have a distinct chemical signature from the background, with peaks in Ti/Ca suggesting a terrestrial source. Riou et al. (2020b) showed that peaks in Ti/Ca were related to volcanic minerals including iddingsite, augite and labradorite. The lack of chemical markers in the other

anomalous layers ($AL1_{16}$, $AL2_{16}$ and $AL3_{16}$) is most probably attributed to the coarser nature of the sediment, with the lack of fine-grained material, such as clay, reflected in low K_{norm} counts, but also low Ti/Ca. However, the near absence of *Halimeda* plates in these anomalous layers, in contrast to their high occurrence in the background sediment, together with the frequently observed bimodal grain size distribution could be related to the mixing of marine and terrestrial material. Alternatively, it cannot be excluded that the near absence of *Halimeda* plates is related to an environmental change less favorable to these algae. While it is less obvious compared to anomalous layers in K08, those identified in K16 are also interpreted to represent event deposits.

Such event deposits (anomalous layers) can be related to large storms or cyclones, which can generate strong waves or flash-floods, but can also be linked to volcanic eruptions or tsunamis (e.g., Tappin, 2007; Sakuna-Schwartz et al., 2015). They can also be interpreted as backwash deposits, based on their grain size change relative to the background sedimentation and higher Ti/Ca, indicating a seaward transport of sediment of terrestrial origin into the marine environment, as also reported in Thailand, Sicily and Portugal, respectively (e.g., Sakuna-Schwartz et al., 2015; Smedile et al., 2020; Feist et al., 2023), and also in Pago Pago Bay, on the south shore of Tutuila (Riou et al., 2020b). Based on the terrigenous signature (higher Ti/Ca related to volcanic minerals, Riou et al.,2020b), the ages, known tsunami waves and cyclones that hit Tutuila Island (Table 1) and similar event layers encountered in a previous study in Pago Pago Bay attributed to recent tsunami backwash deposits following the 2009 South Pacific tsunami and the 1960 Valdivia tsunami (Riou et al., 2020a, 2020b), event layers AL1 to AL5 can be either interpreted as tsunami backwash deposits or cyclone-related flash-flood deposits (Srinivasalu et al., 2010; Sakuna et al., 2012; Pongpiachan et al., 2013; Veerasingam et al., 2014; Sakuna-Schwartz et al., 2015). As pointed out by Tamura et al. (2015), there are still no proxy kits allowing to distinguish tsunami backwash deposits from flash flood deposits and the attribution of a deposit to one or the other origin (tsunami vs flashflood) often relies on the chronological control. Nevertheless, sedimentological characteristics might provide insights into the depositional process.

The grain-size distributions of the anomalous layers display poor to very poor sorting in both cores and a bimodal trend in core K16. According to Sakuna-Schwartz et al. (2015), flash-flood deposits can be characterized by a finer grain size when compared to tsunami backwash deposits. More specifically flash-flood deposits were found to display a very good grain size sorting (Sakuna-Schwartz et al., 2015), whereas backwash tsunami deposits are usually poorly sorted and may sometimes display a bimodal grain size trend (Paris et al., 2007; Tappin, 2007). Feist et al. (2023) also reported poor sorting of event layers attributed to tsunamis on the Algarve Shelf. While Fujiwara and Kamataki (2007) used the occurrence of a stacking pattern of sub-layers as evidence for deposition associated with long period waves (tsunamis), as opposed to storms, such stacking pattern was not observed at our study sites, and also appears to be only seldom reported. Thus, $AL1_{08 \text{ and } 16}$, $AL2_{08 \text{ and } 16}$, $AL3_{08 \text{ and } 16}$, $AL4_{08 \text{ and } 16}$ and possibly $AL5_{16}$ anomalous layers were probably emplaced during tsunami backwash events, although only a comparison of tsunami backwash and flash-flood deposits at the same site might allow a more definite distinction, as the characteristics of these deposits are often site-specific, as also reported around American Samoa (Riou et al., 2020b; this study). Furthermore, the grain size distribution of the source material is likely to have an influence on that of the deposits, while hydrodynamic processes during the deposition of the anomalous layers will also impact their sedimentological characteristics, as will the distance between the source material and the area of deposition.

6.2 Event deposits and proposed source events

The $^{210}Pb_{ex}$-derived age model, corroborated by ^{137}Cs and ^{14}C data, allowed dating of the anomalous layers and correlation between cores K08 and K16 (Figs. 3 – 5). Following their correlation, anomalous layers are labeled event layers (Fig. 5). For each event layer, the estimated age corresponds to the date at the top of the layer.

6.2.1 Event layer EL1

EL1, which is the shallowest event layer, is found in both cores ($AL1_{08}$ and $AL1_{16}$). It is dated to 2009 ± 0.5 CE in core K08 and 2009 ± 0.4 CE in core K16, and most likely corresponds to the 2009 South Pacific Tsunami deposits. Given chronological constraints related to ^{210}Pb and ^{137}Cs activities, it is likely that the plant debris, at the top of $AL1_{08}$, are reworked material. EL1 is thick (5 and 13 cm in $AL1_{08}$ and $AL1_{16}$, respectively) and is characterized by a coarser grain size (than the background sediment) in core K16, but finer in K08 and associated with an increase in K_{norm} and Ti/Ca. In Pago Pago Bay, the tsunami backwash deposit of the 2009 event was also a few cm thick (2 to 7 cm, Riou et al., 2020b) with a strong terrestrial chemical signature (such as Ti/Ca; Fig. 5) (Riou et al., 2020b). Thus, here we provide the first report of tsunami backwash deposits in different depositional environments, associated with a recent event all around an island.

Just below the ^{137}Cs activity peak, which is a reference point for 1964-1965 CE, $AL2_{08}$ and $AL2_{16}$ are observed in both cores. The occurrence of the ^{137}Cs activity peak (1964-1965 CE) immediately below event layer $AL1_{08}$ (in core K08, Fig. 3) suggests that the marine sediment deposited since 1964-1965 CE must have been eroded, possibly by the landward tsunami wave in 2009, as also reported off the coast of NE Japan following the 2011 Tohoku-oki tsunami by Seike et al. (2013). Alternatively, the occurrence of the ^{137}Cs activity peak immediately below event layer $AL1_{08}$ could be explained by a lower sedimentation rate related to higher energy offshore Fagafue Bay.

An alternative origin for the deposits might have been one of the cyclones that affected Tutuila in 1990 and 1991 (Table 1) (WACOP, 2023). While dispersed clasts associated with a higher Ti/Ca in one core of Pago Pago Bay were tentatively attributed to one of these cyclones, also based on ^{210}Pb dating (Riou et al., 2020b), here, the chronology based on ^{210}Pb dating and ^{137}Cs activity suggests that EL1 was emplaced two decades later (around 2009), thus not supporting an event that occurred early 1990. As mentioned above, it might however also due to erosion by the landward tsunami wave in 2009 that would have removed any trace of an earlier event.

6.2.2 Event layer EL2

Event layer EL2 is dated to 1957 ± 1.3 CE in core K08 ($AL2_{08}$) and 1960 ± 2.3 CE in core K16 ($AL2_{16}$). Two hypotheses can be proposed for the event responsible for this anomalous layer: the 1960 Valdivia tsunami or the 1957 Aleutian tsunami. Following the 1960 Valdivia tsunami caused by a 9.5 Mw earthquake, waves and inundations were reported across most of the Southern Pacific (NGDC, 2023). However, despite the main E to W motion of the waves (e.g., Goff et al., 2022) no inundation was reported in the northern bays of Tutuila (NGDC, 2023). There are three reports of runup in Tutuila; two are from Pago Pago, with one based on a tidal gauge report (0.8 m wave amplitude) and the other based on an eyewitness record (2.4 m wave height). The third report is from Fagaalu, near the entrance to Pago Pago Bay and was based on an eyewitness record (0.8 m wave height; NGDC, 2023). Thus, the absence of any other record might simply be due to the lack of instrumental and/or eyewitness record elsewhere on Tutuila.

The 1957 Aleutian tsunami impacted less severely the islands in the southern Pacific (NGDC, 2023). However, probably due to the N to S waves motion, a 1.5 m wave was reported in Fagasa (eyewitness account; NGDC, 2023), just a few km E from Fagafue Bay, and there were also a tide gauge report (0.2 m wave amplitude) and an eyewitness account (1.2 m wave height) in Pago Pago (NGDC, 2023). Therefore, EL2 may correspond either to the 1960 Valdivia or the 1957 Aleutian tsunami deposits, with the chronology not allowing to distinguish one from the other. An event deposit tentatively attributed to the 1960 Valdivia tsunami was reported onshore in Ma'asina, on the N coast of Upolu, Samoa (Williams et al., 2020), as there was a record of waves impacting around the area (Pararas-Carayanis and Dong, 1980). The 1957 Aleutian tsunami was not proposed as an alternative by Williams et al. (2020), possibly because the wave height was much smaller, as reported by Pararas-Carayanis and Dong (1980). Modeling suggests that the Samoan Islands (Samoa and American Samoa) have been impacted by both events (National Oceanic and Atmospheric Administration, 2017), with runup records for the northern coasts of the islands (Pararas-Carayanis and Dong, 1980; NGDC, 2023). However, research carried out in the Hawaiian Islands has shown that the onshore deposits associated

with the 1957 Aleutian tsunami are only a few cm thick at the most, despite runup heights over 10 m (Chagué-Goff et al., 2012; La Selle et al., 2020). While the thickness of tsunami deposits depends on a number of factors, including sediment availability, accommodation space and preservation potential (e.g., Dawson and Stewart, 2007; Szczuciński, 2020), it is likely that no deposit caused by the 1957 event was left behind in the Samoan Islands. In both cores, EL2 is a very thin and discrete layer characterized only by a short Ti/Ca and K_{norm} peak in core K08 and by a slightly coarser mean grain size in core K16. In Pago Pago, the 1960 tsunami backwash deposit was also described as a thin layer characterized by increases in Ti/Ca and other terrestrial chemical signatures (Ti/Sr, Zr/Ca, Zn/Ca, Pb/Ca; Riou et al., 2020b, their Fig. 5). Thus, EL2 is most likely attributed to the 1960 Valdivia tsunami, providing the first report of tsunami backwash deposits associated with an historic event all around an island, similar to what has been observed for the recent 2009 event (Section 6.2.1).

6.2.3 Event layer EL3

EL3 is found only in core K16 ($AL3_{16}$) and is dated to 1920 ± 5.1 CE. Based on the chronological control, it most likely corresponds to the 1917 Tonga Trench tsunami generated by the 8.3 Mw Tonga Trench earthquake (e.g., Okal et al., 2011). It is characterized by a bimodal grain-size distribution, with the presence of a second coarser mode in addition to the fine background marine sediment mode, most probably due to sediment influx from the land, resulting in a sharp mean grain size increase. A deposit potentially associated with the 1917 tsunami has also been reported in Falealupo, on the NW tip of Savaii Island (Samoa) as well as at a few locations on the southern shores of Upolu, Samoa (Williams et al., 2020). Thus, our study provides another datapoint as geological evidence for the 1917 Tonga Trench tsunami in the South Pacific.

6.2.4 Event layer EL4

The chronology in core K16 suggests that the next event layer ($AL4_{16}$) most probably occurred after 1433-1677 CE (based on ^{14}C dating). One possible tsunami source for this event layer could be the

1868 CE Arica Chile tsunami, generated by a Mw 8.5 earthquake offshore the Peru-Chile border (NGDC, 2023), which caused damage in Apia, Samoa (Pararas-Carayanis and Dong, 1980) with eyewitness reports of waves of up to 3 m in Apia and less than 1 m in a few other locations on the northern shore of Upolu (NGDC, 2023). Modeling of the tsunami (Goff et al., 2022) confirms the path of the tsunami waves towards New Zealand and the Samoan Islands. While sedimentological evidence for this event has mostly been found in New Zealand, on the Chatham Islands (Goff et al., 2010; Nichol et al., 2010) and the South Island (Donnelly et al., 2017; Kain et al., 2017), Williams et al. (2020) also reported a possible tsunami deposit in Maasina (northern shore of Upolu) associated with the 1868 CE event (based on ^{210}Pb dating). Thus, the 1868 CE Arica tsunami might represent a possible candidate for the source of $AL4_{16}$ in core K16.

Other alternatives for the source of $AL4_{16}$ in core K16 are older tsunamis possibly from the 14th to 18th century. Two possible known events are the 1604 CE tsunami, generated by a M 8.5 earthquake in Peru (near the epicenter of the 1868 CE Arica earthquake), and the 1575 CE tsunami, caused by a M 8.5 earthquake in Valdivia, Chile (near the epicenter of the 1960 Valdivia earthquake; Lomnitz, 1970; Goff et al., 2010). Deposits associated with the 1604 CE event have been found onshore in New Zealand, including the Chatham Islands (Goff et al., 2010). Modeling suggests that the 1604 CE tsunami might have affected the Samoan Islands (Goff et al., 2022), although the modeled wave amplitude in that region is lower than that of the 1868 CE event. While the thickness of backwash deposits depends on many factors, and not only the wave amplitude and the magnitude of the generating earthquake (or other event), layer $AL4_{16}$ is over 25 cm thick, with a pronounced terrestrial signature that decreases upward. Therefore, a larger event (than the 1604 CE or 1575 CE events) might be more plausible.

One such event is the prehistoric 15th century tsunami, which has been associated with many deposits and archaeological evidence across the South Pacific, although age ranges sometimes extend to the 16th century (see Goff et al., 2022 for a review), with modeling of a Mw 9.4 earthquake on the central Tonga trench showing the wide potential impact of the generated tsunami in the region (Goff et al.,

2022). These authors did not explain why they chose a Mw 9.4 earthquake as the tsunami source for the model, and the magnitude of the event might be overestimated. Although some authors have suggested the source of the earthquake might be on the Tonga Trench, there is still some debate about the source of the 15th century regional tsunami (Lavigne et al., 2021; Goff et al., 2022; Paris et al., 2023). Nevertheless, boulders of coral limestone that were found 30 m a.m.s.l. and 20 m a.m.s.l. in Tonga were linked with a 15th century large tsunami (Lavigne et al., 2021), although Frohlich et al. (2009) suggested a volcanic flank collapse or undersea landslides as the possible cause for these boulders on Tonga. A layer of bioclastic sands at one site on Grande Terre Island, and a layer of pumice lapilli at a site on Maré Island in New Caledonia have also been associated with a 15th century tsunami (Paris et al., 2023). Geological evidence for this event linked with archeological data has been reported from Ofu Island (American Samoa) located about 100 km E of Tutuila (Quintus et al., 2015), and as indicated above, in many other locations in the South Pacific, including Wallis and Futuna (Goff et al., 2011), New Zealand and possibly Australia (Goff et al., 2022). The 15th century tsunami would also match the event that resulted in the anomalous layer $AL3_{08}$ in core K08, which is bracketed between 1416-1663 CE (immediately above the layer) and 1464-1751 CE (immediately below the layer; based on ^{14}C dating) (Fig. 3). While there appears to be an inversion, the ages overlap around 1464-1663 CE, thus corroborating the suggestion of a 15th (or 16th) century tsunami.

Whether the backwash deposits are due to a far-field tsunami or a local tsunami is difficult to ascertain. In the literature, there are hardly any records of backwash deposits at the same site linked with both far-field tsunamis and local tsunamis. The backwash deposit in Pago Pago Bay associated with the 1960 Valdivia tsunami caused by an earthquake about 10,000 km away and that linked with the local 2009 South Pacific tsunami (Fig. 5) (Riou et al., 2020b) are, as far as the authors are aware, the only ones. In Pago Pago Bay, the backwash deposits of the far-field 1960 Valdivia tsunami (no more than 2-3 cm thickness) were thinner than that of the local 2009 South Pacific tsunami (up to 7-8 cm thickness) (Fig. 5) (Riou et al., 2020b). While both deposits were observed in a number of cores in that bay, more evidence from other sites elsewhere in the world and associated with other tsunamis

would be required to be able to draw definite conclusions between the distance of the generating event and the thickness of the backwash deposit, as the latter depends on many other factors, including sediment availability, tsunami wave characteristics, geomorphology and preservation potential, amongst others. Nevertheless, our data, based on the wide occurrence of deposits of a similar age around the Pacific, suggest that event layer EL4, which is recorded in both core K08 ($AL3_{08}$) and K16 ($AL4_{16}$) as deposits of 14 cm and 26.5 cm thickness, respectively, was most probably associated with a large $15^{th}/16^{th}$ century tsunami possibly generated in the South Pacific.

6.2.5 Event layer EL5

The lowest anomalous layer in core K08 ($AL4_{08}$) (Fig. 3) can possibly be linked with the lowest anomalous layer in core K16 ($AL5_{16}$) (Fig. 4). The chronological control based on ^{14}C dating suggests that these layers were deposited prior to 1433-1677 CE (core K16) but after 1031-1290 CE (core K08) (Figs. 3-5). Williams et al. (2020) have tentatively attributed an onshore deposit at Lano, on Savaii, Samoa to a 1100-1300 CE tsunami, whose generating event is unknown. Two large earthquakes resembling the 1960 Valdivia earthquake, and which resulted in large tsunamis, have also been reported to have occurred sometime between about 900-1128 CE and 1300-1398 CE, respectively, about 200 km south of Valdivia, in Chile (Cisternas et al., 2017) and could also potentially represent a source for the event layer EL5. The uncertainty of the dating control does not allow us to be more definite as to the age of the generating event and more work would be required to ascertain the age and source of the tsunami.

Based on relatively well-constrained radiochronology, geochemical and grain size data, together with correlations with already identified backwash deposits (Riou et al., 2020b) (Fig. 5), it is likely that AL1 and AL2 deposited offshore Massacre-Fagafue-Sita Bays and AL1, AL2 and AL3, deposited in Masefau Bay are related to known historic tsunamis, namely the 2009 South Pacific tsunami, the 1960 Valdivia tsunami and the 1917 Tonga Trench tsunami. Given the oldest event (AL3 and AL4 offshore Massacre-Fagafue-Sita Bays, and AL4 and AL5 in Masefau Bay) are less well constrained by radiochronology and

are not correlated to well-documented events, their interpretation as tsunami backwash deposits remains more hypothetical. However, it remains true that they show strong similarities with well-known and recent tsunami backwash deposits.

7. Conclusions

In this study, we present the geological record of tsunamis that have impacted the northern shores of Tutuila Island (American Samoa) based on the analyses of two cores collected offshore the open bay off Fagafue and in the sheltered bay of Masefau. Despite the different hydrodynamic settings between the two study areas, five event layers were identified based on sedimentological, grain-size distributions and geochemical criteria and interpreted as shallow marine tsunami backwash deposits. ^{137}Cs activities, ^{210}Pb and radiocarbon dating throughout the cores allowed correlation of these event deposits between both cores. The three most recent event layers are linked to known historic tsunamis, namely the 2009 South Pacific tsunami, the 1960 Valdivia tsunami and the 1917 Tonga Trench tsunami, the latter being only recorded in the sheltered bay (Masefau). The event layers are mostly characterized by darker sediment with a mean grain size coarsening induced by a bimodal distribution in Masefau Bay. This coarser grain size mode reveals the presence of a coarser terrestrial sediment input transported seaward by the tsunami backwash and is supported by lower amounts of *Halimeda* plates and slight increases in Ti/Ca, although the chemical signature is blurred by the coarser sediment distribution. Offshore Fagafue Bay, the event layers are characterized by finer sediment, and clear increases in Ti/Ca and K_{norm}, reflecting the input of terrestrial material. The fourth event layer was most likely emplaced by a tsunami in the 15-16th century, whose source is still a matter of debate. The oldest event layer corresponds to an event that occurred between the 11th and 14th century, possibly due to a large earthquake in Chile, although more research would be needed to provide more certainty about this event.

Together with backwash deposits of the 2009 South Pacific tsunami and 1960 Valdivia Chile tsunami previously identified in Pago Pago Bay, this study provides the first correlation around an island of

offshore tsunami backwash deposits from two specific events from both a local and a far-field source. This study also provides the first backwash evidence of a large 15th century tsunami, which can be correlated with many onshore evidence (geological, archeological and societal) in other islands of the Pacific, as well as that of a possible event in the 11th-14th century. This work demonstrates the good preservation potential for tsunami backwash deposits below the fair-weather wave base, both in sheltered shallow marine environments and more open bays. It also shows that characteristics of backwash deposits vary in areas separated by short distances (a few kilometers), thus suggesting that more research should be carried out to identify tsunami backwash deposits in the geological record.

Acknowledgments

This paper is based on Brieuc Riou's PhD thesis. Funding for this study was provided by the CNRS-INSU "Risques et catastrophes telluriques" program and the Conseil Régional de la Région Poitou Charentes. ^{210}Pb and ^{137}Cs measurements were self-financed by Sabine Schmidt (EPOC). We thank the Commission Nationale de la Flotte Côtière, the captain Jean-François Barazer and the *R/V Alis* crew members during the SAMOA-SPT oceanographic cruise, the diver John Butscher, as well as Bruce Jaffe (USGS) for his help coordinating and making possible the field survey. We acknowledge all the members of the EPOC core analysis platform Isabelle Billy, the late Pascal Lebleu, Marie-Claire Perello and Olivier Ther, GIS expert Vincent Hanquiez and interns Johanna Juppin and Laurine Monier. We thank Thierry Guyot (LIENSs) for his valuable help for figure improvement. We would also like to thank the two anonymous reviewers, reviewer Dave Tappin and the editor Massimo Moretti for constructive comments that helped improve the manuscript.

References

Apotsos, A., Gelfenbaum, G., Jaffe, B., Watt, S., Peck, B., Buckley, M., Stevens, A., 2011. Tsunami inundation and sediment transport in a sediment-limited embayment on American Samoa. Earth-Science Reviews 107, 1–11.

Blott, S., Pye, K., 2001. GRADISTAT: a grainsize distribution and statistics package for the analysis of unconsolidated sediments. Earth Surface Processes and Landforms 26, 1237-1248.

Chagué, C., 2020. Applications of geochemical proxies in paleotsunami research. In: Engel, M., Pilarczyk, J., May, S.M., Brill, D., Garrett, E. (Eds.), Geological Records of Tsunamis and Other Extreme Waves. Elsevier, Amsterdam, The Netherlands, pp. 381-401.

Chagué-Goff, C., Schneider, J.-L., Goff, J.R., Dominey-Howes, D., Strotz, L., 2011. Expanding the proxy toolkit to help identify past events — Lessons from the 2004 Indian Ocean Tsunami and the 2009 South Pacific Tsunami. Earth-Science Reviews 107, 107–122.

Chagué-Goff, C., Goff, J., Nichol, S.L., Dudley, W., Zawadzki, A., Bennett, J.W., Mooney, S.D., Fierro, D., Heijnis, H., Dominey-Howes, D., Courtney, C., 2012. Multi-proxy evidence for trans-Pacific tsunamis in the Hawai'ian Islands. Marine Geology 299-302, 77-89.

Chagué-Goff, C., Szczuciński, W., Shinozaki, T., 2017. Applications of geochemistry in tsunami research: A review. Earth-Science Reviews 165, 203–244.

Cisternas, M., Garrett, E., Wesson, R., Dura, T., Ely, L.L., 2017. Unusual geologic evidence of coeval seismic shaking and tsunamis shows variability in earthquake size and recurrence in the area of the giant 1960 Chile earthquake. Marine Geology 385, 101-113.

Collard, F., Ardhuin, F., Chapron, B., 2009. Monitoring and analysis of ocean swell fields from space: New methods for routine observations. Journal of Geophysical Research 114, C07023, doi:10.1029/2008JC005215

Costa, P.J.M., Andrade, C., Dawson, S., 2015. Geological recognition of onshore tsunami deposits. In: Finkl, C.W., Makowski, C. (Eds.), Environmental Management and Governance. Springer International Publishing, Cham, pp. 3–32.

Cuven, S., Paris, R., Falvard, S., Miot-Noirault, E., Benbakkar, M., Schneider, J.-L., Billy, I., 2013. High-resolution analysis of a tsunami deposit: Case-study from the 1755 Lisbon tsunami in southwestern Spain. Marine Geology 337, 98-111.

Dawson, A.G., Stewart, I., 2007. Tsunami deposits in the geological record. Sedimentary Geology 200, 166–183.

Donnelly, J., Goff, J., Chagué-Goff, C., 2017. A record of local storms and trans-Pacific tsunamis, eastern Banks Peninsula, New Zealand. The Holocene 27, 496-508.

Feist, L., Costa, P.J.M., Bellanova, P., Bosnic, I., Santisteban, J.I., Andrade, C., Brückner, H., Duarte, J.F., Kuhlmann, J., Schwarzbauer, J., Vött, A., Reicherter, K., 2023. Holocene offshore tsunami archive – Tsunami deposits on the Algarve shelf (Portugal). Sedimentary Geology 448, 106369 https://doi.org/10.1016/j.sedgeo.2023.1063692

Fritz, H.M., Borrero, J.C., Synolakis, C.E., Okal, E.A., Weiss, R., Titov, V.V., Jaffe, B.E., Foteinis, S., Lynett, P.J., Chan, I.-C., Liu, P.L.-F., 2011. Insights on the 2009 South Pacific tsunami in Samoa and Tonga from field surveys and numerical simulations. Earth-Science Reviews 107, 66–75.

Frohlich, C., Hornbach, M.J., Taylor, F.W., Shen, C.-C., Moala, A., Morton, A.E., Kruger, J., 2009. Huge erratic boulders in Tonga deposited by a prehistoric tsunami. Geology 37, 131-134.

Fujiwara, O., Kamataki, T., 2007. Identification of tsunami deposits considering the tsunami waveform: An example of subaqueous tsunami deposits in Holocene shallow bay on southern Boso Peninsula, Central Japan. Sedimentary Geology 200, 295–313.

Goff, J., Nichol, S., Chagué-Goff, C., Horrocks, M., McFadgen, B., Cisternas, M., 2010. Predecessor to New Zealand's largest historic trans-South Pacific tsunami of 1868AD. Marine Geology 275, 155–165.

Goff, J., Lamarche, G., Pelletier, B., Chagué-Goff, C., Strotz, L., 2011. Predecessors to the 2009 South Pacific tsunami in the Wallis and Futuna archipelago. Earth-Science Reviews 107, 91-106.

Goff, J., Borrero, J., Easton, G., 2022. In search of Holocene trans-Pacific palaeotsunamis. Earth-Science Reviews 233, 104194 https://doi.org/10.1016/j.earscirev.2022.104194

Hancock, G., Leslie, C., Everett, S., Tims, S., Brunskill, G., Haese, R., 2011. Plutonium as a chronomarker in Australian and New Zealand sediments: a comparison with 137 Cs. Journal of Environmental Radioactivity 102, 919-929.

Hawkins, J.W., Natland, J.H., 1975. Nephelinites and basanites of the Samoan linear volcanic chain: Their possible tectonic significance. Earth and Planetary Science Letters 24, 427–439.

Heaton, T.J., Köhler, P., Butzin, M., Bard, E., Reimer, R.W., Austin, W.E.N., Bronk Ramsey, C., Grootes, P.M, Hughen, K.A, Kromer, B., Reimer, P.J., Adkins, J., Burke, A., Cook, M.S., Olsen, J., Skinner, L.C., 2020. Marine20 - the marine radiocarbon age calibration curve (0–55,000 cal BP). Radiocarbon 62, 779 - 820

Ikehara, K., Irino, T., Usami, K., Jenkins, R., Omura, A., Ashi, J., 2014. Possible submarine tsunami deposits on the outer shelf of Sendai Bay, Japan resulting from the 2011 earthquake and tsunami off the Pacific coast of Tohoku. Marine Geology 356, 120–127.

Ikehara, K., Kanamatsu, T., Nagahashi, Y., Strasser, M., Fink, H., Usami, K., Irino, T., Wefer, G., 2016. Documenting large earthquakes similar to the 2011 Tohoku-oki earthquake from sediments deposited in the Japan Trench over the past 1500 years. Earth and Planetary Science Letters 445, 48-56.

Ikehara, K., Usami, K., Kanamatsu, T., 2020. Repeated occurrence of surface-sediment remobilization along the landward slope of the Japan Trench by great earthquakes. Earth, Planets and Space 72, 114, doi:10.1186/s40623-020-01241-y

Ikehara, K., Usami, K., Irino, T., Omura, A., Jenkins, R.G., Ashi, J., 2021. Characteristics and distribution of the event deposits induced by the 2011 Tohoku-oki earthquake and tsunami offshore of Sanriku and Sendai, Japan. Sedimentary Geology 411, 105791, https://doi.org/10.1016/j.sedgeo.2020.105791.

Jaffe, B.E., Gelfenbaum, G., Buckley, M.L., Watt, S., Apotsos, A., Stevens, A.W., Richmond, B.M., 2010. The limit of inundation of the September 29, 2009, tsunami on Tutuila, American Samoa. U. S. Geological Survey. Open-File_Report 2010-1018, 31 pp.

Johnson, J.M., Tanioka, Y., Ruff, L.J., Satake, K., Kanamori, H., Sykes, L.R., 1994. The 1957 great Aleutian earthquake. Pure and Applied Geophysics 142, 3–28.

Kain, C., Wassmer, P., Goff, J., Chagué-Goff, C., Gomez, C., Hart, D., Fierro, D., Jacobsen, G., Zawadzki, A., 2017. Determining flow patterns and emplacement dynamics from tsunami deposits with no visible sedimentary structure. Earth Surface Processes and Landforms 42, 763-780.

Keys, J.G., 1963. The tsunami of 22 May 1960, in the Samoa and Cook Islands. Bulletin of the Seismological Society of America 53, 1211-1227.

Koppers, A.A.P., Russell, J.A., Jackson, M.G., Konter, J., Staudigel, H., Hart, S.R., 2008. Samoa reinstated as a primary hotspot trail. Geology 36, 435-438.

Krishnaswamy, S., Lal, D., Martin, J., Meybeck, M., 1971. Geochronology of lake sediments. Earth and Planetary Science Letters 11, 407-414.

Kümmerer, V., Drago, T., Veiga-Pires, C., Silva, P.F., Magalhães, V., Mena, A., Lopes, A., Rodrigues, A.I., Schmidt, S., Terrinha, P., 2020. Exploring offshore sediment evidence of the 1755 CE Tsunami (Faro, Portugal): Implications for the study of outer shelf tsunami deposits. Minerals 10, 731. doi:10.3390/min10090731

La Selle, S., Richmond, B.M., Jaffe, B.E., Nelson, A.R., Griswold, F.R., Arcos, M.E.M., Chagué, C., Bishop, J.M., Bellanova, P., Kane, H.H., Lunghino, B.D., Gelfenbaum, G., 2020. Sedimentary evidence of prehistoric distant-source tsunamis in the Hawaiian Islands. Sedimentology 67, 1249-1273.

Lavigne, F., Morin, J., Wassmer, P., Weller, O., Kula, T., Maea, A.V., Kelfoun, K., Mokadem, F., Paris, R., Malawani, M.N., 2021. Bridging legends and science: field evidence of a large tsunami that affected the Kingdom of Tonga in the 15th Century. Frontiers in Earth Science 9, 748755 , doi: 10.3389/feart.2021.748755.

Lomnitz, C., 1970. Major earthquakes and tsunamis in Chile during the period 1535 to 1955. Geologische Rundschau 59, 938-960.

Morrison, R.J., Peshut, P.J., Lasorsa, B.K., 2010. Elemental composition and mineralogical characteristics of coastal marine sediments of Tutuila, American Samoa. Marine Pollution Bulletin 60, 925–930.

National Geophysical Data Center (NGDC) / World Data Service: NCEI/WDS Global Historical Tsunami Database, 2023. NOAA National Centers for Environmental Information. doi:10.7289/V5PN93H7 (last accessed 21 April 2023).

National Oceanic and Atmospheric Administration (NOAA)/Tsunami historical series, 2017. Aleutian Islands, 1957. https://sos.noaa.gov/catalog/datasets/tsunami-historical-series-aleutian-islands-1957/

Natland, J.H., 1980. The progression of volcanism in the Samoan linear volcanic chain. American Journal of Science 280, 709–735.

Nichol, S., Chagué-Goff, C., Goff, J., Horrocks, M., McFadgen, B., Strotz, L., 2010. Geomorphology and accommodation space as limiting factors on tsunami deposition: Chatham Island, southwest Pacific Ocean. Sedimentary Geology 229, 41-52.

Okal, E.A., Borrero, J.C., Chagué-Goff, C., 2011. Tsunamigenic predecessors to the 2009 Samoa earthquake. Earth-Science Reviews 107, 128–140.

Pararas-Carayannis, G., Dong, B., 1980. Catalog of Tsunamis in the Samoan Islands. International Tsunami Information Center, Honolulu, 75 pp.

Paris, R., Lavigne, F., Wassmer, P., Sartohadi, J., 2007. Coastal sedimentation associated with the December 26, 2004 tsunami in Lhok Nga, west Banda Aceh (Sumatra, Indonesia). Marine Geology 238, 93–106.

Paris, R., Pelletier, B., Roger, J., Wassmer, P., Sabatier, P., 2023. Sedimentary evidence of tsunamis in New Caledonia, southwest Pacific. Marine Geology, 107116 https://doi.org/10.1016/j.margeo.2023.107116

Petchey, F., Anderson, A., Zondervan, A., Ulm, S., Hogg, A., 2008. New marine ΔR values for the South Pacific subtropical gyre region. Radiocarbon 50, 373–397.

Pongpiachan, S., Thumanu, K., Tanthanuch, W., Tipmanee, D., Kanchai, P., Schwarzer, K., Tancharakorn, S., 2013. Sedimentary features of tsunami backwash deposits as assessed by micro-beam synchrotron X-ray fluorescence (μ-SXRF) at the Siam photon laboratory. Journal of Tsunami Society International 32, 96–115.

Quintus, S., Clark, J.T., Day, S.S., Schwert, D.P., 2015. Landscape evolution and human settlement patterns on Ofu Island, Manu'a Group, American Samoa. Asian Perspectives 54, 208-237.

Reimer, R.W. Reimer, P.J. 2023 CALIBomb [WWW program] at http://calib.org (accessed 18 December 2023).

Riou, B., 2019. Shallow Marine Sediment Record of Tsunamis: Analysis of the Sediment-Fill of the Bays of Tutuila (American Samoa) and Backwash Deposits of the 2009 South Pacific Tsunami (Ph.D. thesis). Rochelle Université, La Rochelle.

Riou, B., Chaumillon, E., Schneider, J.-L., Corrège, T., Chagué, C., 2020a. The sediment-fill of Pago Pago Bay (Tutuila Island, American Samoa): New insights on the sediment record of past tsunamis. Sedimentology 67, 1577-1600.

Riou, B., Chaumillon, E. Chagué, C., Sabatier, P., Schneider, J.-L., Walsh, J.-P., Zawadzki, A., Fierro, D., 2020b. Backwash sediment record of the 2009 South Pacific Tsunami and 1960 Great Chilean Earthquake Tsunami. Scientific Reports 10, 4149. https://doi.org/10.1038/s41598-020-60746-4

Sakuna, D., Szczuciński, W., Feldens, P., Schwarzer, K., Khokiattiwong, S., 2012. Sedimentary deposits left by the 2004 Indian Ocean tsunami on the inner continental shelf offshore of Khao Lak, Andaman Sea (Thailand). Earth, Planets and Space 64, 931–943.

Sakuna-Schwartz, D., Feldens, P., Schwarzer, K., Khokiattiwong, S., Stattegger, K., 2015. Internal structure of event layers preserved on the Andaman Sea continental shelf, Thailand: tsunami vs. storm and flash-flood deposits. Natural Hazards and Earth System Science 15, 1181–1199.

Schmidt, S., De Deckker, P., 2015. Present-day sedimentation rates on the southern and southeastern Australian continental margins. Australian Journal of Earth Sciences 62, 143-150.

Schneider, J.-L., 2015. SAMOA-SPT cruise, RV Alis, https://doi.org/10.17600/15004100

Seike, K., Shirai, K., Kogure, Y., 2013. Disturbance of shallow marine soft-bottom environments and megabenthos assemblages by a huge tsunami induced by the 2011 M9.0 Tohoku-Oki earthquake. PLoS One 8, e65417, https://doi.org/10.1371/journal.pone.0065417

Seike, K., Kitahashi, T., Noguchi, T., 2016. Sedimentary features of Onagawa Bay, northeastern Japan after the 2011 off the Pacific coast of Tohoku Earthquake: sediment mixing by recolonized benthic animals decreases the preservation potential of tsunami deposits. Journal of Oceanography *72*, 141-149.

Smedile, A., Molisso, F., Chagué, C., Iorio, M., De Martini, P.M., Pinzi, S., Collins, P.E.F., Sagnotti, L., Pantosti, D., 2020. New coring study in Augusta Bay expands understanding of offshore tsunami deposits (Eastern Sicily, Italy). Sedimentology 67, 1553-1576.

Srinivasalu, S., Jonathan, M.P., Thangadurai, N., Ram-Mohan, V., 2010. A study on pre- and post-tsunami shallow deposits off SE coast of India from the 2004 Indian Ocean tsunami: a geochemical approach. Natural Hazards 52, 391-401.

Stuiver, M., Reimer, P.J., 1993. CALIB rev. 8. Radiocarbon 35, 215-230.

Szczuciński, W., 2020. Post-depositional changes to tsunami deposits and their preservation potential. In: Engel, M., Pilarczyk, J., May, S.M., Brill, D., Garrett, E. (Eds.), Geological Records of Tsunamis and Other Extreme Waves. Elsevier, Amsterdam, The Netherlands, pp. 443-469.

Tamura, T., Sawai, Y., Ikehara, K., Nakashima, R., Hara, J., Kanai, Y., 2015. Shallow-marine deposits associated with the 2011 Tohoku-oki tsunami in Sendai Bay, Japan. Journal of Quaternary Science 30, 293-297.

Tappin, D.R., 2007. Sedimentary features of tsunami deposits—Their origin, recognition and discrimination: An introduction. Sedimentary Geology 200, 151-154.

Terry, J.P., Kostaschuk, R.A., Garimella, S., 2006. Sediment deposition rate in the Falefa River basin, Upolu Island, Samoa. Journal of Environmental Radioactivity 86, 45-63.

Veerasingam, S., Venkatachalapathy, R., Basavaiah, N., Ramkumar, T., Venkatramanan, S., Deenadayalan, K., 2014. Identification and characterization of tsunami deposits off southeast

coast of India from the 2004 Indian Ocean tsunami: Rock magnetic and geochemical approach. Journal of Earth System Science 123, 905–921.

WACOP (Waves & Coasts in the Pacific), 2023. Wave Climate Report Pago Pago. http://gsd.spc.int/wacop/. [accessed 12 November 2023]

Weiss, R., Bahlburg, H., 2006. A note on the preservation of offshore tsunami deposits. Journal of Sedimentary Research 76, 1267–1273.

Williams, S., Prasetya, G., Chagué-Goff, C., Goff, J., Cheung, K.F., Davies, T., Wilson, T., 2011a. Characterising diagnostic proxies for identifying palaeotsunamis in a tropical climatic regime, Samoan Islands. In: OCEANS'11 MTS/IEEE KONA. IEEE, pp. 1–10.

Williams, S.P., Goff, J.R., Sale, F., Ah Kau, J., Prasetya, G., Davies, T.R., Cheung, K.F., Wilson, T., 2011b. Sands of Time: Evidence for palaeotsunamis and/or palaeostorms in Samoa, and what this means for tsunami risk reduction. In: Proceedings of the Samoa National Environment Forum, pp. 15–25.

Williams, S., Titimaea, A., Bosserelle, C., Simanu, L., Prasetya, G., 2020. Reassessment of long-term tsunami hazards in Samoa based on sedimentary signatures. Geosciences 10, 481, doi:10.3390/geosciences10120481

Yoshikawa, S., Kanamatsu, T., Goto, K., Sakamoto, I., Yagi, M., Fujimaki, M., Imura, R., Nemoto, K., Sakaguchi, H., 2015. Evidence for erosion and deposition by the 2011 Tohoku-oki tsunami on the nearshore shelf of Sendai Bay, Japan. Geo-Marine Letters 35, 315-328.

Figure and table captions

Fig. 1 – (a) Location of Samoa and American Samoa in the southwest Pacific (modified from Google, Maxar Technologies). (b) Topographic and bathymetric map of Tutuila (modified from NOAA, 2018; https://data.noaa. gov/dataset/dataset/gridded-bathymetry-of-tutuila-island-american-samoa-south-pacific – acknowledgments to NOAA Coral Reef Ecosystem Division, Pacific Islands Fisheries Science Center and the Pacific Islands Benthic Habitat Mapping Center, School of Ocean and Earth Science and Technology, University of Hawaii). (c) Bathymetric map of Massacre – Fagafue – Sita Bays and locations of coring sites. (d) Bathymetric map of Masefau Bay and locations of coring sites. Bathymetry of maps (c) and (d) was acquired during the SAMOA-SPT (1 m high resolution) and processed with CARAIBES software (IFREMER).

Fig. 2 – Example of samples used radiocarbon dating. (a) Photograph of vascular plant debris sampled in core K08 (134 cm depth, see Table 3 for details). (b) Photograph of *Halimeda* calcified plates sampled in core K16 (82 cm depth, see Table 3 for details). (c) Photograph of *Operculina Ammonoides* sampled in core K08 (69 cm depth, see Table 3 for details).

Fig. 3 – Results of multi-proxy analysis of core K08. From left to right: ages obtained by radiocarbon (^{14}C) and ^{210}Pb dating as well as ^{137}Cs activity, photograph of the core, grain size distribution, mean grain size, Ti/Ca ratio, K_{norm}, excess ^{210}Pb activities, age model and sediment accumulation rate (SAR), and ^{137}Cs and ^{132}Th activities. Gray shaded bars represent anomalous layers $AL1_{08}$, $AL2_{08}$, $AL3_{08}$ and $AL4_{08}$.

Fig. 4 – Results of multi-proxy analysis of core K16. From left to right: ages obtained by radiocarbon (^{14}C) and ^{210}Pb dating as well as ^{137}Cs activity, photograph of the core, grain size distribution, mean grain size, Ti/Ca ratio, K_{norm}, excess ^{210}Pb activities, age model and sediment accumulation rate (SAR), and ^{137}Cs and ^{132}Th activities. Gray shaded bars represent anomalous layers $AL1_{16}$, $AL2_{16}$, $AL3_{16}$, $AL4_{16}$and $AL5_{16}$.

Fig. 5 – Identification of event layers (EL) from the correlation of anomalous layers observed at locations K08 (Fagafue Bay), K16 (Masefau Bay), and Ca08 (Pago Pago Bay, Riou et al., 2020b) cores around the island of Tutuila. The correlation is based on sedimentological and geochemical characteristics, as well as ^{210}Pb and ^{14}C dating, and ^{137}Cs activity. From top to bottom, event layers are interpreted as records of the 2009 South Pacific tsunami (EL1), the 1960 Valdivia tsunami (EL2), the 1917 Tonga Trench tsunami (EL3), one tsunami that occurred during the 15th/16th century (EL4) and one tsunami that occurred between the 11th and 14th century (EL5).

Table 1 - Known tsunamis and cyclones that have affected Tutuila, American Samoa (up to 2015).

Date	Event type	Source (for tsunamis)	Location of Reported Impacts	Impacts	References
2009	Tsunami	Tonga Trench Earthquake	Pola Bay	10 m wave height, 18 m run-up height	Fritz et al. (2011)
			Fagafue Bay	5 m wave height, 12 m run-up height	Fritz et al. (2011)
				250 m inland inundation	Apotsos et al. (2011)
			Masefau Bay	4 m wave height, 5 m run-up height	Fritz et al. (2011)
				7 m flow depth	Apotsos et al. (2011)
				290 m inland inundation	Jaffe et al. (2010)
			Fagasa Bay	10 m wave height	Fritz et al. (2011)
			Pago-Pago Bay	8 m wave height	Fritz et al. (2011)
				500 m inland inundation up Vaipito River	Fritz et al. (2011)

1991	Cyclone Val	WACOP (2023)	Pago-Pago Bay	6.74 m wave height
1990	Cyclone Ofa	WACOP (2023)	Pago-Pago Bay	7.98 m wave height
1960	Tsunami	Valdivia Earthquake NGDC (2023)	Pago-Pago Bay	4 m wave height, 2.4 m run-up height
1957	Tsunami	Aleutian Islands Earthquake NGDC (2023)	Fagasa Bay	1.5 m run-up height
1917	Tsunami	Tonga Trench Earthquake NGDC (2023)	Pago-Pago Bay	2.4 m wave height
1837	Tsunami	Chile Earthquake NGDC (2023)	Pago-Pago Bay	0.60 m wave height

Table 2 – Cores sampled in Masefau Bay and offshore Fagafue Bay. Core code, core type, water depth, location and length of cores are provided.

Core code	Core type	Water depth (m)	Location	Latitude	Longitude	Length (cm)
K08	Kullenberg core	50	Fagafue Bay	S14°16.973	W170°45.334	144
K09	Kullenberg core	50	Fagafue Bay	S14°16.925	W170°45.585	157
K10	Kullenberg core	65	Fagafue Bay	S14°16.703	W17045.787	259
P04.1	Manual core	23	Fagafue Bay	S14°17.425	W10°45.173	14
P04.2	Manual core	23	Fagafue Bay	S14°17.425	W10°45.173	12
P04.3	Manual core	20	Fagafue Bay	S14°17.425	W10°45.173	7
K15	Kullenberg core	44.5	Masefau Bay	S14°15.188	W170°37.364	144
K16	Kullenberg core	44.5	Masefau Bay	S14°15.164	W170°37.343	150
K17	Kullenberg core	55	Masefau Bay	S14°15.108	W170°37'166"	186
P05.1	Manual core	37	Masefau Bay	S14°15.290	W170°37.403	16
P05.2	Manual core	37	Masefau Bay	S14°15.290	W170°37.403	14

Table 3 - Radiocarbon data in cores K08 and K16. Sample ID, Laboratory ID, Depth (cm), material sampled, Conventional ages (years BP or pMC), calibrated ages (2 σ).

Core	Sample	Lab #	Depth (cm)	Material	Conventional age (years BP)	Calibrated age (years CE) (2 σ)
K08	SPT20	Poz-112047	13	Plant debris	120.77 ± 0.35 pMC	1960-1962–1985-1987 CE
K08	SPT21	Poz-112048	69	Foraminifera	830 ± 30	1416-1663 CE
K08	SPT22	Poz-107478	83	*Halimeda* plates	740 ± 30	1464-1751 CE
K08	SPT23	Poz-112049	125	Foraminifera	1260 ± 30	1031-1290 CE
K16	SPT24	Poz-107473	82	*Halimeda* plates	300 ± 35	-
K16	SPT25	Poz-112050	125	*Halimeda* plates	805 ± 30	1433-1677 CE

Table 4 – Description of the anomalous layers (AL).

Anomalous Layer #	Depth (cm)	Sediment description	Mean grain size range (μm)	Sorting range	Skewness range	Kurtosis range	XRF	Organic remains
$AL1_{08}$	13-18	unimodal, poorly to very poorly sorted sandy mud normal grading	72-137	113-192	2.48-5.18	10.14-36.37	increase in K_{norm} Higher Ti/Ca ratio	vascular plant debris at top
$AL2_{08}$	23.5-26	unimodal, very poorly sorted sandy mud (without any grading)	86-94	122-132	2.85-3.12	12.62-14.85	marked increase in K_{norm} at base, higher K_{norm} counts and Ti/Ca ratio	
$AL3_{08}$	71-85	unimodal, very poorly sorted sandy mud + muddy sand at the base and top Normal grading then reverse grading	45-158	68-260	2.08-4.41	7.64-28.22	gradual increase in Ti/Ca and K_{norm} at the base	
$AL4_{08}$	103.5-112.5	alternation of bimodal and unimodal poorly to very poorly sorted muddy sand	98-332	132-467	1.74-4.28	4.99-27.72	increase in Ti/Ca	
$AL1_{16}$	7-20	dark very poorly sorted muddy sand displaying an alternation of layers with bimodal and unimodal grain size distribution	125-390	146-503	1.03-2.80	3.45-11.39	Ti/Ca does not exhibit any changes with the underlying sediment /	rare *Halimeda* plates

							small marked decrease at the upper boundary	
$AL2_{16}$	35.5-40	trimodal, bimodal and unimodal poorly to very poorly sorted sandy mud with muddy sand at the top (inverse grading)	64-253	00-377	2.07-4.36	7.01-26.34	Ti/Ca and K_{norm} do not display any major changes from the background	few *Halimeda* plates
$AL3_{16}$	60-75	very poorly sorted sandy mud and muddy sand with a sharp base	99-364	153-462	1.39-2.93	4.24-13.07	Ti/Ca and K_{norm} do not display any major changes from the background	few *Halimeda* plates
$AL4_{16}$	93-119.5	bimodal very poorly sorted sandy mud with thin intercalations of muddy sand + sharp basal contact	88-299	161-385	1.42-3.09	4.92-13.16	very high Ti/Ca and K_{norm} + sharp increase at the base	few *Halimeda* plates
$AL5_{16}$	135-139.5	bimodal very poorly sorted sandy mud + finer than the background	82-324	149-354	1.34-3.056	4.35-12.46	small peak in both Ti/Ca	

and
K_{norm}

Declaration of interests

☒ The authors declare that they have no known competing financial interests or personal relationships that could have appeared to influence the work reported in this paper.

☐ The authors declare the following financial interests/personal relationships which may be considered as potential competing interests:

Brieuc Riou reports financial support was provided by La Rochelle University. Brieuc Riou reports a relationship with La Roche University that includes: funding grants.

Highlights

First geological evidence for backwash deposits of two tsunamis around an island

Terrestrial geochemical signature in backwash deposits

Backwash deposits associated with up to five historic and prehistoric tsunamis

Record of tsunami backwash deposits extends back to 11th-14th century

Possible evidence for 15th-16th century tsunami

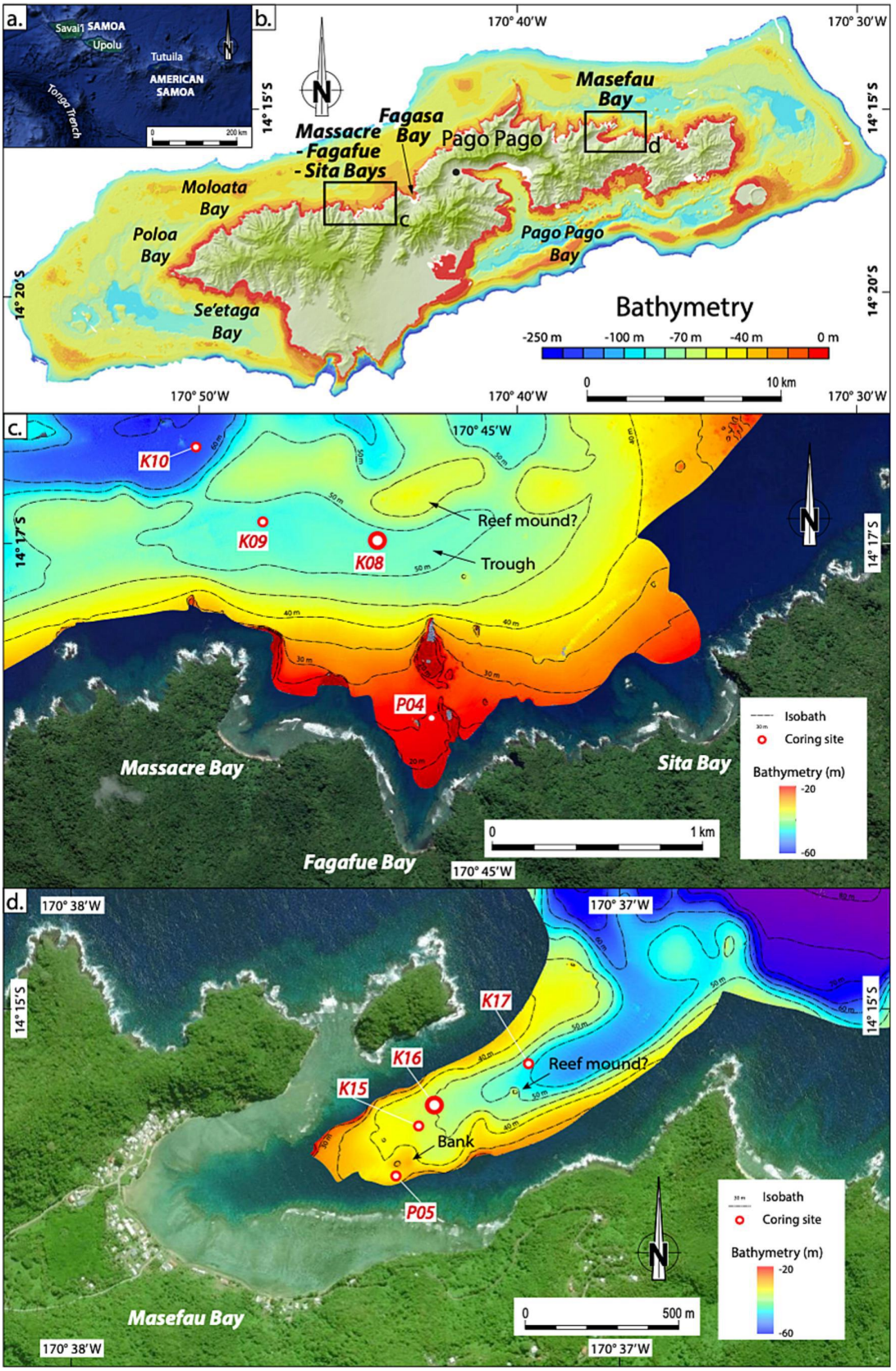
a.
Savai'i
SAMOA
Upolu
Tutuila
AMERICAN SAMOA
Tonga Trench
0
200 km
b.
170° 40'W
170° 30'W
14° 15'S
14° 20'S
N
Masefau Bay
Fagasa Bay
Massacre - Fagafue - Sita Bays
Pago Pago
d
c
Moloata Bay
Poloa Bay
Pago Pago Bay
Se'etaga Bay
Bathymetry
-250 m
-100 m
-70 m
-40 m
0 m
0
10 km
170° 50'W
c.
170° 45'W
14° 17'S
K10
K09
K08
Reef mound?
Trough
P04
Massacre Bay
Sita Bay
Fagafue Bay
Isobath
Coring site
Bathymetry (m)
-20
-60
0
1 km
d.
170° 38'W
170° 37'W
K17
K16
K15
Reef mound?
Bank
P05
Masefau Bay
0
500 m

Figure 1

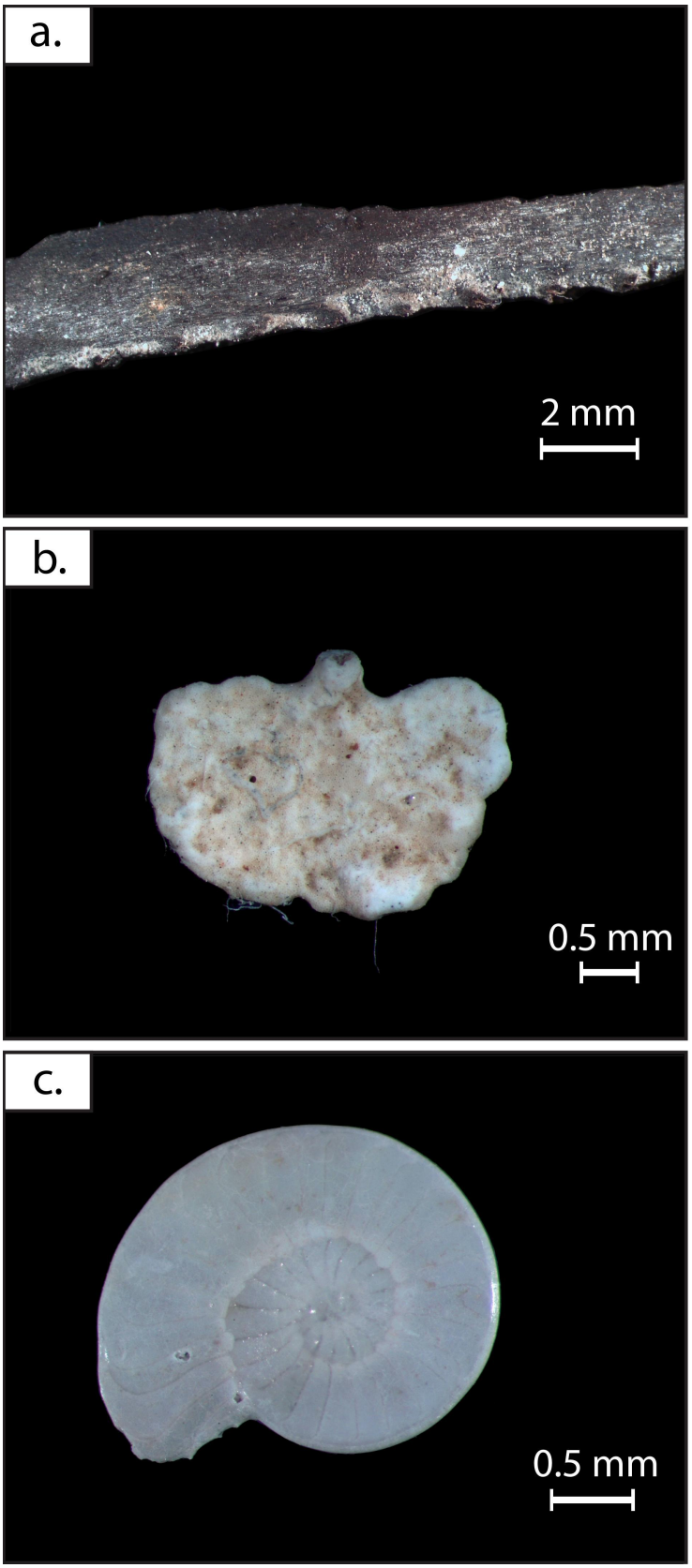

Figure 2

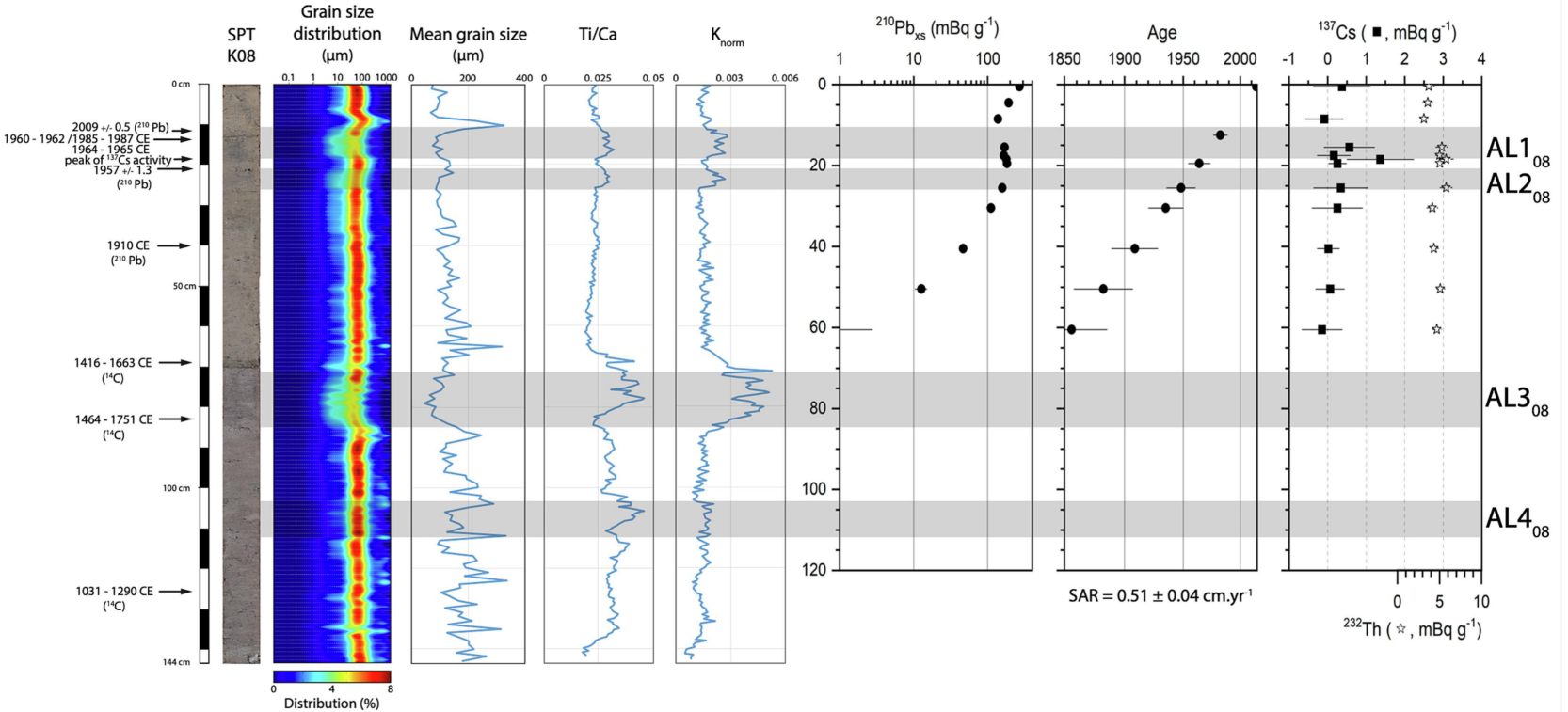
SPT K08
Grain size distribution (µm)
Mean grain size (µm)
Ti/Ca
K norm
210Pbxs (mBq g-1)
Age
137Cs (■, mBq g-1)
0 cm
2009 +/- 0.5 (210 Pb)
1960 - 1962 /1985 - 1987 CE
1964 - 1965 CE
peak of 137Cs activity
1957 +/- 1.3
(210 Pb)
1910 CE
(210 Pb)
50 cm
1416 - 1663 CE
(14C)
1464 - 1751 CE
(14C)
100 cm
1031 - 1290 CE
(14C)
144 cm
Distribution (%)
AL1 08
AL2 08
AL3 08
AL4 08
SAR = 0.51 ± 0.04 cm.yr-1
232Th (☆, mBq g-1)

Figure 3

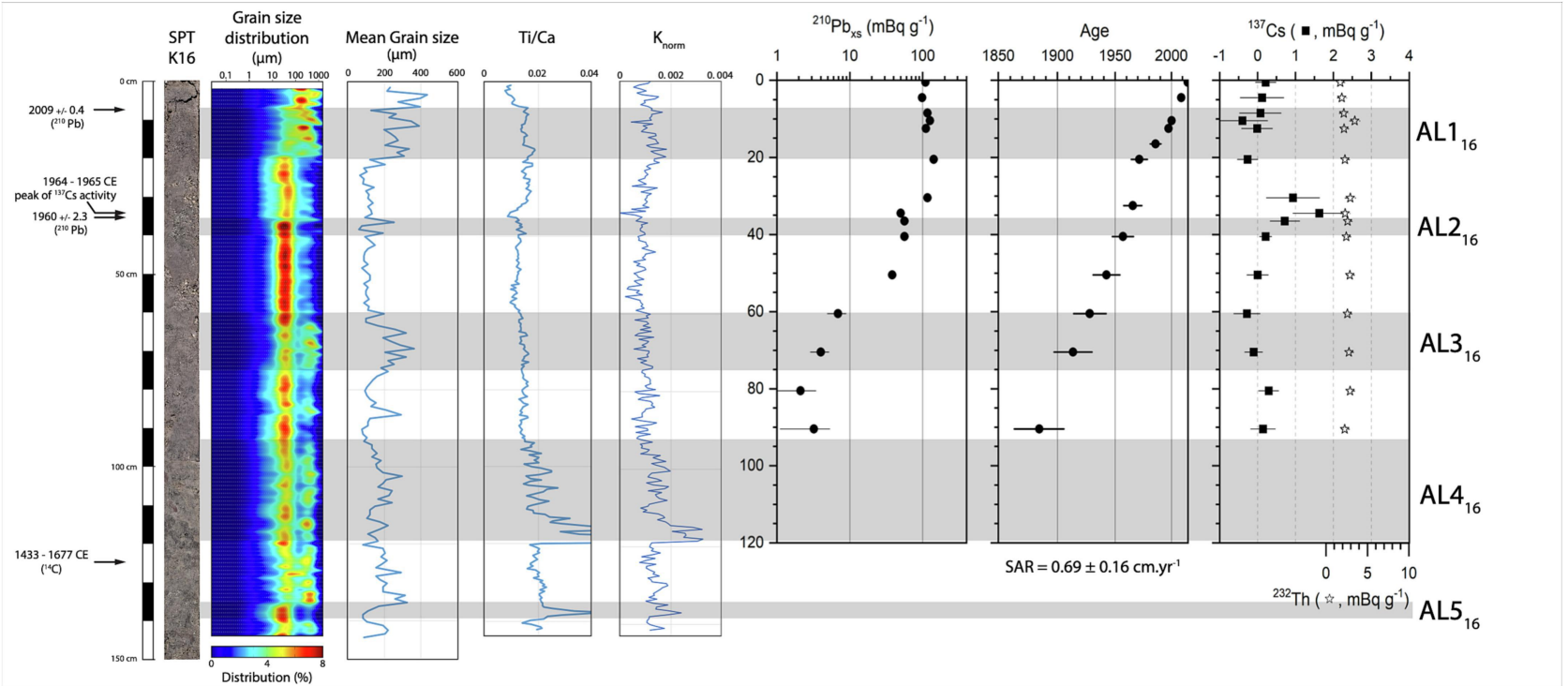
SPT K16
Grain size distribution (µm)
Mean Grain size (µm)
Ti/Ca
K_norm
210Pb_xs (mBq g-1)
Age
137Cs (■ , mBq g-1)
2009 +/- 0.4 (210 Pb)
1964 - 1965 CE peak of 137Cs activity
1960 +/- 2.3 (210 Pb)
1433 - 1677 CE (14C)
Distribution (%)
SAR = 0.69 ± 0.16 cm.yr-1
232Th (☆ , mBq g-1)
AL1 16
AL2 16
AL3 16
AL4 16
AL5 16

Figure 4

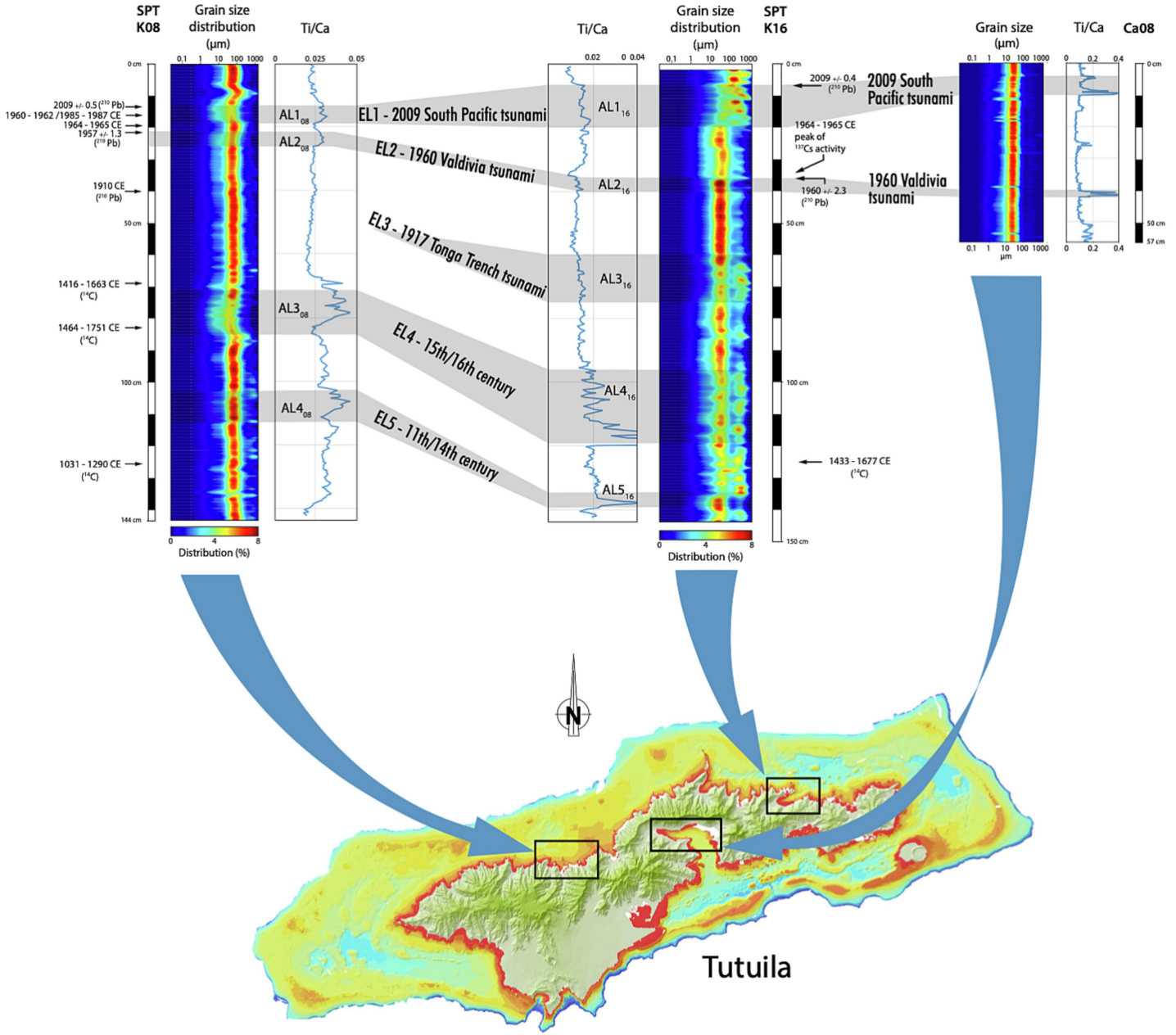
SPT K08
Grain size distribution (µm)
Ti/Ca
Ti/Ca
Grain size distribution (µm)
SPT K16
Grain size (µm)
Ti/Ca
Ca08
2009 +/- 0.5 (210 Pb)
1960 - 1962 /1985 - 1987 CE
1964 - 1965 CE
1957 +/- 1.3 (210 Pb)
1910 CE (210 Pb)
1416 - 1663 CE (14C)
1464 - 1751 CE (14C)
1031 - 1290 CE (14C)
AL1 08
AL2 08
AL3 08
AL4 08
EL1 - 2009 South Pacific tsunami
EL2 - 1960 Valdivia tsunami
EL3 - 1917 Tonga Trench tsunami
EL4 - 15th/16th century
EL5 - 11th/14th century
AL1 16
AL2 16
AL3 16
AL4 16
AL5 16
2009 +/- 0.4 (210 Pb)
1964 - 1965 CE peak of 137Cs activity
1960 +/- 2.3 (210 Pb)
1433 - 1677 CE (14C)
2009 South Pacific tsunami
1960 Valdivia tsunami
Distribution (%)
Distribution (%)
µm
N
Tutuila

Figure 5